Multi-time-step explicit-implicit method for non-linear structural dynamics

Anthony Gravouil, Alain Combescure

Multi-time-step explicit–implicit method for non-linear structural dynamics

Anthony Gravouil[†;‡] and Alain Combescure[§,¶]

Laboratoire de Mécanique et Technologie; ENS de Cachan; 61 Avenue du President Wilson; 94235 Cachan Cedex; France

We present a method with domain decomposition to solve time-dependent non-linear problems. This method enables arbitrary numeric schemes of the Newmark family to be coupled with different time steps in each subdomain: this coupling is achieved by prescribing continuity of velocities at the interface. We are more specifically interested in the coupling of implicit=explicit numeric schemes taking into account material and geometric non-linearities. The interfaces are modelled using a dual Schur formulation where the Lagrange multipliers represent the interfacial forces. Unlike the continuous formulation, the discretized formulation of the dynamic problem is unable to verify simultaneously the continuity of displacements, velocities and accelerations at the interfaces. We show that, within the framework of the Newmark family of numeric schemes, continuity of velocities at the interfaces enables the definition of an algorithm which is stable for all cases envisaged. To prove this stability, we use an energy method, i.e. a global method over the whole time interval, in order to verify the algorithms properties. Then, we propose to extend this to non-linear situations in the following cases: implicit linear=explicit non-linear, explicit non-linear=explicit non-linear and implicit non-linear=explicit non-linear. Finally, we present some examples showing the feasibility of the method.

KEY WORDS: non-linear structural dynamics; multi-time-step method; mixed method; subcycling; dual Schur domain decomposition method

1. INTRODUCTION

Explicit time integration for transient problems discretized in space using finite elements is very widespread, particularly for contact or impact problems, or when wave propagation effects are important [1, 2]. Explicit methods allow the implementation of complex models with a limited calculation cost, and the conditional stability of these algorithms is not a problem if the time step necessary for the required precision is in the order of the critical time step

*Correspondence to: Alain Combescure, Laboratoire de Mecanique et Technologie, Ecole Normale Superierure de Cachan, 61 Avenue du President Wilson, 94235 Cachan Cedex, France
† Research student
‡ E-mail: gravouil@lmt.ens-cachan.fr
§ Professor
¶ E-mail: combescure@lmt.ens-cachan.fr

[3, 4]. However, if the meshes have widely different element sizes (or material properties), the smallest element in the structure sets the time step for the whole structure. This situation arises, for example, in coupled fluid/structure problems or in h-type adaptive meshing techniques. In 1977, Belytschko and Mullen [5] proposed a multi-time-step (or subcycling) integration method involving different time steps in different zones of the model. This approach differs from the mixed methods in time [6–8] which consist of defining zones where different time integration techniques apply, but with a single time step defined for the whole structure. One can also attempt to couple two approaches, 'mixed method' and 'subcycling' [9].

Mixed method in time: Three types of methods are generally found—'explicit/explicit', 'explicit/implicit' and 'implicit/implicit' algorithms [10, 11]. In all three cases, one distinguishes element-partitioning methods from node-partitioning methods. Thus, for example, one may consider two subdomains laid out according to the nodes or according to the elements. This distinction is important for the interface because each of the methods is specific in the way the interface is treated. Besides, in the three cases E/E, E/I and I/I, the numeric scheme in time is constructed as follows: we assume a Newmark numeric scheme with two characteristic parameters β, γ identical for all subdomains. The distinction between 'explicit' and 'implicit' thus refers to regions where we have considered, respectively, a diagonal (explicit) or a consistent (implicit) mass matrix [9]. 'Explicit/implicit' methods with the same time step are used primarily for hyperbolic problems. One of the first algorithms with nodal partitioning was proposed in [12] and its stability with a non-symmetric amplification matrix was studied in [6]. A first method with element partitioning was proposed in [7], and the study of its stability with a symmetric amplification matrix using an energy method was done in Reference [8]. Non-linear applications can be found especially in References [13, 14]. There is also an extension to the HHT method in Reference [15] along with a proof of stability by Fourier's method with a displacement, velocity and acceleration state vector. Furthermore, a variation on these methods was proposed in Reference [16] whereby, the inside of the subdomains is implicit and the boundary explicit.

Multi-time-step methods in time (*subcycling*): Again, two main classes of algorithms apply to these methods: element partitioning and nodal partitioning. If we disregard mixed methods in time with subcycling at this stage, these methods have been used mainly for implicit cases. But, this time, the numeric scheme considered for the whole structure is 'explicit' in the sense that $\beta = 0$ in the Newmark numeric scheme (with a diagonal mass matrix). The first method with multi-time-step was proposed in Reference [17], with nodal partitioning for second-order explicit/implicit systems and linearly interpolated displacements at the interface, but with no general stability proof. A first proof of stability for first-order systems using the energy method can be found in Reference [18], but with highly restrictive assumptions which limit applications. Subsequently, stability conditions were proposed [19] for explicit first-order systems with element partitioning. A generalization of the previous study to the implicit case was developed in Reference [20] for first-order systems. Then, one can find for the first time in Reference [21] a rigorous and general stability analysis of subcycling with nodal partitioning for parabolic systems. One can also find an explicit multi-time-step integration algorithm for the element-free Galerkin method for diffusion problems in [22]. The stability analysis of multi-time-step integration schemes for second-order systems creates much greater difficulties because the amplification matrix in the case of nodal partitioning is not symmetric. A proof of the stability of such schemes in the explicit case was proposed in [23] with nodal partitioning and a modified explicit scheme [24]. This proof uses

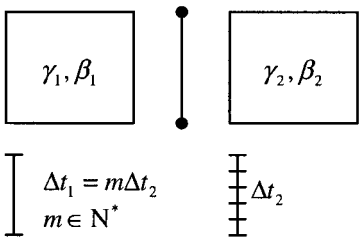

Figure 1. Coupling of arbitrary numeric schemes of the Newmark family with different time steps.

both spectral approach and energy approach. One can find in Reference [25] a variation on these methods for the explicit case, where the adjustment from the coarse time scale to the fine time scale is no longer performed at constant velocity, but at constant acceleration, which seems to help improve the convergence of the algorithm. So far, for second-order systems other than explicit/explicit, there has been no proof of stability of the subcycling techniques [25].

Mixed- and multi-time-step methods [20]: Under this definition, we consider 'explicit/implicit' methods in the sense of mixed methods in time, i.e. with a single pair of parameters β, γ for the whole structure and a diagonal mass matrix for the explicit part. These algorithms are used for first-order systems in [19] and for second-order systems in References [17, 19]. In the first case, a stability study of the algorithm with subcycling is proposed for the explicit/explicit case, but no extension to the explicit/implicit case with element partitioning is proposed. For second-order systems, as indicated in References [9, 25], there is, at this point, no general stability analysis in the explicit/implicit case with subcycling.

In this presentation, another direction has been considered to couple arbitrary numeric schemes of the Newmark family in each subdomain with different time steps [26, 27] (Figure 1).

To achieve this objective, a dual Schur domain decomposition method was chosen [28–38]. In Section 2, we describe the algorithm in the linear case; then, we perform a numerical stability study using an energy method [8]. In Section 3, we propose an extension of the method to the non-linear case; then, we validate the algorithm through different examples, both linear and non-linear, with large time-step ratios.

2. STUDY OF SUBCYCLING IN HYBRID FORMULATION/LINEAR CASE

2.1. Case of the Newmark family of numeric schemes

The objective of this article is to present a method which, in the context of a dual Schur domain decomposition approach for a dynamic problem, allows one to take into account the specific properties of the different parts of the structure in the time domain. The subdomains considered can have non-linear constitutive relations and large displacements. Thus, generally speaking, the subdomains can be chosen according to the physical phenomena occurring in different parts of the structure. First, we consider a continuous domain Ω with prescribed displacements on $\partial_1\Omega$ and prescribed loads on $\partial_2\Omega$. We assume small perturbations. The

finite element discretization of the continuous problem leads to the following equations:

$$\forall t \in [0,T], \quad \mathbf{M}\ddot{\mathbf{U}} + \mathbf{F}_{\text{int}} = \mathbf{F}_{\text{ext}} \tag{1}$$

where $\mathbf{M}$ represents the symmetric, positive-definite mass matrix, $\ddot{\mathbf{U}}$ the discretized acceleration field, $\mathbf{F}_{\text{int}}$ the discretized internal forces and $\mathbf{F}_{\text{ext}}$ the applied external forces. The following initial conditions and constraints complete the above differential system:

$$\begin{aligned} \mathbf{U}_{|t=0} &= \mathbf{U}_0 \\ \dot{\mathbf{U}}_{|t=0} &= \mathbf{V}_0 \end{aligned} \quad \text{and} \quad \mathbf{U}_{|\partial_1\Omega} = \mathbf{U}_{\text{d}} \tag{2}$$

This type of problem, in general, involves banded sparse matrices because of the finite element discretization. Thus, the bandwidth represents the coupling between the degrees of freedom of the differential system: in this sense, the equilibrium equation is global in space. In order to take advantage of the properties of the explicit and implicit schemes [39], we perform a time discretization using the Newmark family of numeric time schemes [3, 40–44], which allow us to chose either one of the methods depending on two parameters β and γ,

$$\begin{aligned} \mathbf{U}_{n+1} &= {}^{\text{p}}\mathbf{U}_n + \beta\Delta t^2 \ddot{\mathbf{U}}_{n+1} \\ \dot{\mathbf{U}}_{n+1} &= {}^{\text{p}}\dot{\mathbf{U}}_n + \ \Delta t \ddot{\mathbf{U}}_{n+1} \end{aligned} \tag{3}$$

with

$$\begin{aligned} {}^{\text{p}}\mathbf{U}_n &= \mathbf{U}_n + \Delta t \dot{\mathbf{U}}_n + \Delta t^2 \left(\tfrac{1}{2} - \ \right) \ddot{\mathbf{U}}_n \\ {}^{\text{p}}\dot{\mathbf{U}}_n &= \dot{\mathbf{U}}_n + \Delta t (1-\gamma) \ddot{\mathbf{U}}_n \end{aligned} \tag{4}$$

where the time interval $[0,T]$ is discretized as follows: $t_0 < t_1 < \cdots < t_r$ with $r \in \mathbf{N}^*$, $n \in \{1,\ldots,r\}$, $t_0 = 0$, $t_r = T$, r being the number of time intervals Δt assumed constant. $\mathbf{U}_{n+1}$, $\dot{\mathbf{U}}_{n+1}$ and $\ddot{\mathbf{U}}_{n+1}$ represent the unknown displacements, velocities and accelerations at time t_{n+1}, ${}^{\text{p}}\mathbf{U}_n$ and ${}^{\text{p}}\dot{\mathbf{U}}_n$ represent the predictors of the numeric scheme, i.e. the known quantities from the previous time step. We perform the decomposition of the structure into s subdomains following a dual Schur formulation. Thus, the equilibrium of the interface forces is automatically verified through the Lagrange multipliers. Regarding the kinematic quantities, three cases can be envisaged [45]: we can prescribe continuity of displacements, or continuity of velocities, or continuity of accelerations at the interface. Indeed, from a discretized point of view, we cannot enforce the continuity of all kinematic quantities at the interface. Later on, we will show that continuity of the velocities at the interface enables us to address the coupling of arbitrary numeric schemes of the Newmark family with different time steps for each subdomain. The decomposition into subdomains of the differential system (1) can be written as follows:

$$\begin{aligned} &\mathbf{M}^k \ddot{\mathbf{U}}^k + \mathbf{F}^k_{\text{int}} = \mathbf{F}^k_{\text{ext}} + \mathbf{F}^k_{\text{link}}, \quad \forall k \in \{1,\ldots,s\} \\ &\sum_{k=1}^{\text{p}} \mathbf{C}^k \dot{\mathbf{U}}^k = 0 \qquad\qquad \forall t \in [0,T] \end{aligned} \tag{5}$$

with the connecting forces at the interface between subdomains

$$\mathbf{F}^k_{\text{link}} = \mathbf{C}^{k^{\text{T}}} \boldsymbol{\Lambda} \tag{6}$$

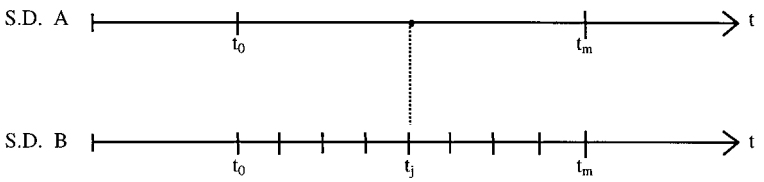

Figure 2. Different time scales for each subdomain A and B.

where $\dot{\mathbf{U}}^k$ represents the discretized velocity field, $\mathbf{C}^k$ the Boolean connectivity matrices for perfect connection between compatible meshes and $\mathbf{\Lambda}$ the vector of Lagrange multipliers. In this first study, we consider a structure made of a linear elastic, homogeneous and isotropic material. Thus,

$$\mathbf{F}_{\text{int}}^k = \mathbf{K}^k \mathbf{U}^k \quad \forall k \in \{1, \ldots, s\} \tag{7}$$

To simplify the problem, let us first consider two subdomains A and B. For example, we can consider an implicit scheme on subdomain A and an explicit scheme on subdomain B. Let us assume that subdomain A is associated with a coarse time scale (time step ΔT) and subdomain B with a fine time scale (time step Δt). We will assume that $\Delta T = m\Delta t$ (Figure 2).

Then, Equations (3)–(6) enable us to write the system of discretized equations in space and in time for our problem on a time step ΔT of the coarse time scale:

$$\tilde{\mathbf{M}}^{\text{A}} \ddot{\mathbf{U}}_m^{\text{A}} = \mathbf{F}_{\text{ext}_m}^{\text{A}} - \mathbf{K}^{\text{A}} \left({}^{\text{p}}\mathbf{U}_0^{\text{A}} \right) + \mathbf{C}^{\text{A}^{\text{T}}} \mathbf{\Lambda}_m \tag{8}$$

$$\tilde{\mathbf{M}}^{\text{B}} \ddot{\mathbf{U}}_j^{\text{B}} = \mathbf{F}_{\text{ext}_j}^{\text{B}} - \mathbf{K}^{\text{B}} \left({}^{\text{p}}\mathbf{U}_{j-1}^{\text{B}} \right) + \mathbf{C}^{\text{B}^{\text{T}}} \mathbf{\Lambda}_j \tag{9}$$

with

$$\mathbf{C}^{\text{A}} \dot{\mathbf{U}}_j^{\text{A}} + \mathbf{C}^{\text{B}} \dot{\mathbf{U}}_j^{\text{B}} = 0 \tag{10}$$

$$\tilde{\mathbf{M}}^{\text{A}} = \mathbf{M}^{\text{A}} + \beta_{\text{A}} \Delta T^2 \mathbf{K}^{\text{A}} \quad \text{and} \quad \tilde{\mathbf{M}}^{\text{B}} = \mathbf{M}^{\text{B}} + \beta_{\text{B}} \Delta t^2 \mathbf{K}^{\text{B}} \tag{11}$$

We can immediately note that the continuity of velocities (10) on the fine time scale requires that the velocity at the edge of subdomain A be evaluated at time t_j. Similarly, Equations (8) and (9) are coupled through the Lagrange multipliers and require that the dual quantities of the edge velocities, i.e. the Lagrange multipliers on the fine time scale, be evaluated. For this purpose, we propose the following transition operators from the fine time scale to the coarse time scale (along the edges of the subdomains):

$$\mathbf{C}^{\text{A}} \dot{\mathbf{U}}_j^{\text{A}} = \left(1 - \frac{j}{m} \right) \mathbf{C}^{\text{A}} \dot{\mathbf{U}}_0^{\text{A}} + \frac{j}{m} \mathbf{C}^{\text{A}} \dot{\mathbf{U}}_m^{\text{A}} \tag{12}$$

$$\mathbf{\Lambda}_j = \left(1 - \frac{j}{m} \right) \mathbf{\Lambda}_0 + \frac{j}{m} \mathbf{\Lambda}_m \tag{13}$$

An interesting way to present the system of Equations (8)–(10) is to divide all unknowns of the problem into an ‘constrained’ group and a ‘constrained’ group. The first category

corresponds to the solution of the equilibrium subdomain by subdomain without taking into account the interface forces. The second category corresponds to correcting terms for the interface forces between subdomains. Thus, the Newmark scheme (3) becomes

$$\begin{aligned} \mathbf{U}_{n+1_{\text{free}}} &= {}^{\text{p}}\mathbf{U}_n + \Delta t^2 \ddot{\mathbf{U}}_{n+1_{\text{free}}} \quad \mathbf{U}_{n+1_{\text{link}}} = \beta \Delta t^2 \ddot{\mathbf{U}}_{n+1_{\text{link}}} \\ \dot{\mathbf{U}}_{n+1_{\text{free}}} &= {}^{\text{p}}\dot{\mathbf{U}}_n + \Delta t \ddot{\mathbf{U}}_{n+1_{\text{free}}} \quad \dot{\mathbf{U}}_{n+1_{\text{link}}} = \gamma \Delta t \ddot{\mathbf{U}}_{n+1_{\text{link}}} \end{aligned} \tag{14}$$

Therefore, we can write for each subdomain an 'unconstrained' problem and a 'constrained' problem:

$$\tilde{\mathbf{M}}^{\text{A}} \ddot{\mathbf{U}}^{\text{A}}_{m_{\text{free}}} = \mathbf{F}^{\text{A}}_{\text{ext}_m} - \mathbf{K}^{\text{Ap}} \mathbf{U}^{\text{A}}_0 \tag{15}$$

$$\begin{pmatrix} \alpha^{\text{A}} \tilde{\mathbf{M}}^{\text{A}} & -\alpha^{\text{A}} \mathbf{C}^{\text{A}^{\text{T}}} \\ -\alpha^{\text{A}} \mathbf{C}^{\text{A}} & 0 \end{pmatrix} \begin{pmatrix} \ddot{\mathbf{U}}^{\text{A}}_{m_{\text{link}}} \\ \boldsymbol{\Lambda}_m \end{pmatrix} = \begin{pmatrix} 0 \\ \mathbf{C}^{\text{A}} \dot{\mathbf{U}}^{\text{A}}_{m_{\text{free}}} + \mathbf{C}^{\text{B}} \dot{\mathbf{U}}^{\text{B}}_{m_{\text{free}}} + \mathbf{C}^{\text{B}} \dot{\mathbf{U}}^{\text{B}}_{m_{\text{link}}} \end{pmatrix} \tag{16}$$

$$\tilde{\mathbf{M}}^{\text{B}} \ddot{\mathbf{U}}^{\text{B}}_{j_{\text{free}}} = \mathbf{F}^{\text{B}}_{\text{ext}_j} - \mathbf{K}^{\text{Bp}} \mathbf{U}^{\text{B}}_{j-1} \tag{17}$$

$$\begin{pmatrix} \alpha^{\text{B}} \tilde{\mathbf{M}}^{\text{B}} & -\alpha^{\text{B}} \mathbf{C}^{\text{B}^{\text{T}}} \\ -\alpha^{\text{B}} \mathbf{C}^{\text{B}} & 0 \end{pmatrix} \begin{pmatrix} \ddot{\mathbf{U}}^{\text{B}}_{j_{\text{link}}} \\ \boldsymbol{\Lambda}_j \end{pmatrix} = \begin{pmatrix} 0 \\ \mathbf{C}^{\text{A}} \dot{\mathbf{U}}^{\text{A}}_{j_{\text{free}}} + \mathbf{C}^{\text{A}} \dot{\mathbf{U}}^{\text{A}}_{j_{\text{link}}} + \mathbf{C}^{\text{B}} \dot{\mathbf{U}}^{\text{B}}_{j_{\text{free}}} \end{pmatrix} \tag{18}$$

with

$$\alpha^{\text{A}} = \gamma_{\text{A}} \Delta T \quad \text{and} \quad \alpha^{\text{B}} = \gamma_{\text{B}} \Delta t \tag{19}$$

The last step consists of expressing the problem condensed on the interface on the fine time scale. This also requires that we decouple the scale change operator (12). Thus, we obtain

$$\begin{aligned} \mathbf{C}^{\text{A}} \dot{\mathbf{U}}^{\text{A}}_{j_{\text{free}}} &= \left(1 - \frac{j}{m}\right) \mathbf{C}^{\text{A}} \dot{\mathbf{U}}^{\text{A}}_{0_{\text{free}}} + \frac{j}{m} \mathbf{C}^{\text{A}} \dot{\mathbf{U}}^{\text{A}}_{m_{\text{free}}} \\ \mathbf{C}^{\text{A}} \dot{\mathbf{U}}^{\text{A}}_{j_{\text{link}}} &= \left(1 - \frac{j}{m}\right) \mathbf{C}^{\text{A}} \dot{\mathbf{U}}^{\text{A}}_{0_{\text{link}}} + \frac{j}{m} \mathbf{C}^{\text{A}} \dot{\mathbf{U}}^{\text{A}}_{m_{\text{link}}} \end{aligned} \tag{20}$$

From (20b) and (16), we get

$$\mathbf{C}^{\text{A}} \dot{\mathbf{U}}^{\text{A}}_{j_{\text{link}}} = \left(1 - \frac{j}{m}\right) \alpha^{\text{A}} \mathbf{C}^{\text{A}} \tilde{\mathbf{M}}^{\text{A}^{-1}} \mathbf{C}^{\text{A}^{\text{T}}} \boldsymbol{\Lambda}_0 + \frac{j}{m} \alpha^{\text{A}} \mathbf{C}^{\text{A}} \tilde{\mathbf{M}}^{\text{A}^{-1}} \mathbf{C}^{\text{A}^{\text{T}}} \boldsymbol{\Lambda}_m \tag{21}$$

Finally, Equation (13) leads to

$$\mathbf{C}^{\text{A}} \dot{\mathbf{U}}^{\text{A}}_{j_{\text{link}}} = \alpha^{\text{A}} \mathbf{C}^{\text{A}} \tilde{\mathbf{M}}^{\text{A}^{-1}} \mathbf{C}^{\text{A}^{\text{T}}} \boldsymbol{\Lambda}_j \tag{22}$$

This enables us to reformulate the matrix system (18) expressed on the fine scale:

$$\begin{pmatrix} \alpha^{\text{B}} \tilde{\mathbf{M}}^{\text{B}} & -\alpha^{\text{B}} \mathbf{C}^{\text{B}^{\text{T}}} \\ -\alpha^{\text{B}} \mathbf{C}^{\text{B}} & -\alpha^{\text{A}} \mathbf{C}^{\text{A}} \tilde{\mathbf{M}}^{\text{A}^{-1}} \mathbf{C}^{\text{A}^{\text{T}}} \end{pmatrix} \begin{pmatrix} \ddot{\mathbf{U}}^{\text{B}}_{j_{\text{link}}} \\ \boldsymbol{\Lambda}_j \end{pmatrix} = \begin{pmatrix} 0 \\ \mathbf{C}^{\text{A}} \dot{\mathbf{U}}^{\text{A}}_{j_{\text{free}}} + \mathbf{C}^{\text{B}} \dot{\mathbf{U}}^{\text{B}}_{j_{\text{free}}} \end{pmatrix} \tag{23}$$

This leads to the problem condensed at the interfaces on the fine time scale

$$\mathbf{H} \boldsymbol{\Lambda}_j = -\left(\mathbf{C}^{\text{A}} \dot{\mathbf{U}}^{\text{A}}_{j_{\text{free}}} + \mathbf{C}^{\text{B}} \dot{\mathbf{U}}^{\text{B}}_{j_{\text{free}}}\right) \tag{24}$$

① solve the "unconstrained" problem of subdomain A at time t_m	see (14) and (15)
② loop on the m time steps of subdomain B at times t_j	
③ solve the "unconstrained" problem of subdomain B	see (14) and (17)
④ change time scale at the edge of subdomain A	see (20a)
⑤ calculate the Lagrange multipliers	see (24)
⑥ solve the "constrained" problem of subdomain B	see (18)
⑦ calculate the kinematic quantities of subdomain B	$(\ ) \equiv (\ )_{\text{free}} + (\ )_{\text{link}}$
⑧ if $j=m$, then end loop	
⑨ solve the "constrained" problem of subdomain A	see (16)
⑩ calculate the kinematic quantities of subdomain A	$(\ ) \equiv (\ )_{\text{free}} + (\ )_{\text{link}}$

Figure 3. Flow-chart of the new mixed- and multi-time-step method.

① initialize the time "markers" for each subdomain	$t_k = 0 \quad \forall k \in \{1,...,s\}$ and $t = 0$
② loop on time steps Δt of the fine scale	$t = t + \Delta t$
③ loop on the s subdomains	
if $t_k < t$, then $t_k = t_k + \Delta t_k$ and solve the unconstrained problem	
if $t_k \neq t$, interpolate the unconstrained velocities	
④ end loop on subdomains	
⑤ solve the condensed problem at the interfaces	
⑥ loop on the s subdomains	
if $t_k = t$, then solve the constrained problem	
⑦ end loop on subdomains	
⑧ end loop on time steps of the fine scale	

Figure 4. Flow-chart of the new mixed- and multi-time-step method with s subdomains.

with

$$\mathbf{H} = \left(\alpha^{\mathrm{A}}\mathbf{C}^{\mathrm{A}}\tilde{\mathbf{M}}^{\mathrm{A}^{-1}}\mathbf{C}^{\mathrm{A}^{\mathrm{T}}} + \alpha^{\mathrm{B}}\mathbf{C}^{\mathrm{B}}\tilde{\mathbf{M}}^{\mathrm{B}^{-1}}\mathbf{C}^{\mathrm{B}^{\mathrm{T}}}\right) \tag{25}$$

Finally, we can present the method for a time step ΔT in the form of the following algorithm (Figure 3):

The method can be generalized to s subdomains with the assumption

$$\begin{aligned} &\Delta t_1 = \Delta t \\ &\Delta t_2 = m_2 \Delta t \quad \text{with } \{m_2, \ldots, m_s\} \in \mathrm{N}^{*s-1} \\ &\ldots \\ &\Delta t_s = m_s \Delta t \end{aligned} \tag{26}$$

The generalized algorithm takes the following form (Figure 4):

Conclusions: The condensation operator on the interfaces depends on the different time steps associated with each subdomain. However, if these are constant (which is generally the case in linear analysis), the condensation operator (25) remains constant during the analysis throughout the time interval $[0, T]$. Therefore, it can be factorized only once at the onset of the dynamic calculation.

This algorithm enables the coupling of any Newmark numeric scheme with a different time step in each subdomain. The continuity of velocities plays a fundamental role in this approach,

and the linear interpolation of velocities (12) allows us to preserve the global stability of the algorithm. The proof is done in the next section.

2.2. Stability and convergence study

The purpose of this study is to show that continuity of the velocities at the interface results in a stable algorithm which makes possible the coupling of numeric schemes of the Newmark family with different time steps. The stability study is performed using an energy method [8]. Thereafter, we will use the following notations:

$$\langle \mathbf{X}_j \rangle = (\mathbf{X}_j + \mathbf{X}_{j+1})/2 \quad \text{and} \quad \lfloor \mathbf{X}_j \rfloor = (\mathbf{X}_{j+1} - \mathbf{X}_j) \tag{27}$$

$$\langle\langle \mathbf{X}_0 \rangle\rangle = (\mathbf{X}_0 + \mathbf{X}_m)/2 \quad \text{and} \quad [\![\mathbf{X}_0]\!] = (\mathbf{X}_m - \mathbf{X}_0) \tag{28}$$

The energy expression associated with subdomain A is defined by

$$[\![T^{\mathrm{A}}(\ddot{\mathbf{U}}_0^{\mathrm{A}})]\!] + [\![V^{\mathrm{A}}(\dot{\mathbf{U}}_0^{\mathrm{A}})]\!] = -D^{\mathrm{A}}([\![\ddot{\mathbf{U}}^{\mathrm{A}}]\!]) + E^{\mathrm{A}}_{\mathrm{interface}}([\![\dot{\mathbf{U}}_0^{\mathrm{A}}]\!], [\![\mathbf{\Lambda}_0]\!]) \tag{29}$$

with

- $T(\ddot{\mathbf{U}}) = \frac{1}{2}\,\ddot{\mathbf{U}}^{\mathrm{T}}\mathbf{A}\ddot{\mathbf{U}}$, term associated with the kinetic energy
- $V(\dot{\mathbf{U}}) = \frac{1}{2}\,\dot{\mathbf{U}}^{\mathrm{T}}\mathbf{K}\dot{\mathbf{U}}$, term associated with the internal energy
- $D(\ddot{\mathbf{U}}) = \left(\ -\frac{1}{2}\right)\ddot{\mathbf{U}}^{\mathrm{T}}\mathbf{A}\ddot{\mathbf{U}}$, term associated with the numerical damping
- $E^{\mathrm{A}}_{\mathrm{interface}}(\dot{\mathbf{U}}, \mathbf{\Lambda}) = \frac{1}{\Delta t}\dot{\mathbf{U}}^{\mathrm{T}}\mathbf{C}^{\mathrm{T}}\mathbf{\Lambda}$, term associated with the work of connecting forces

where matrix $\mathbf{A}$ is defined by

$$\mathbf{A} = \mathbf{M} + \frac{\Delta t^2}{2}(2\beta - \gamma)\mathbf{K} \tag{30}$$

Remark. We do not take the term associated with the work of external forces into account, since this term does not affect the stability of the numeric scheme [9].

Similarly, let us recall expression (29) applied to subdomain B on the time interval $[t_0, t_m]$

$$[\![T^{\mathrm{B}}(\ddot{\mathbf{U}}_0^{\mathrm{B}})]\!] + [\![V^{\mathrm{B}}(\dot{\mathbf{U}}_0^{\mathrm{B}})]\!] = -\sum_{j=1}^{m} D^{\mathrm{B}}([\ddot{\mathbf{U}}_{j-1}^{\mathrm{B}}]) + \sum_{j=1}^{m} \frac{1}{\Delta t}[\dot{\mathbf{U}}_{j-1}^{\mathrm{B}}]^{\mathrm{T}}\mathbf{C}^{\mathrm{B}^{\mathrm{T}}}[\mathbf{\Lambda}_{j-1}] \tag{31}$$

with the notation

$$\sum_{j=1}^{m} [\mathbf{A}_{j-1}] = [\![\mathbf{A}_0]\!] \tag{32}$$

Finally, in order to study the stability of the algorithm, we can apply the energy method to the complete structure, i.e. to both subdomains A and B and to their interface:

$$([\![T^{\mathrm{A}}]\!] + [\![T^{\mathrm{B}}]\!]) + ([\![V^{\mathrm{A}}]\!] + [\![V^{\mathrm{B}}]\!]) = -D^{\mathrm{A}} - \sum_{j=1}^{m} D^{\mathrm{B}}([\ddot{\mathbf{U}}_{j-1}^{\mathrm{B}}]) + E_{\mathrm{link}} \tag{33}$$

with the interface term

$$E_{\mathrm{interface}} = E^{\mathrm{A}}_{\mathrm{interface}} + E^{\mathrm{B}}_{\mathrm{interface}} = \frac{1}{m\Delta t}[\![\dot{\mathbf{U}}_0^{\mathrm{A}}]\!]^{\mathrm{T}}\mathbf{C}^{\mathrm{A}^{\mathrm{T}}}[\![\mathbf{\Lambda}_0]\!] + \sum_{j=1}^{m} \frac{1}{\Delta t}[\dot{\mathbf{U}}_{j-1}^{\mathrm{B}}]^{\mathrm{T}}\mathbf{C}^{\mathrm{B}^{\mathrm{T}}}[\mathbf{\Lambda}_{j-1}] \tag{34}$$

Then, we try to achieve the condition

$$E_{\text{interface}} \leqslant 0 \tag{35}$$

which expresses the fact that the stability of the different schemes is not affected by the interface. We also need an adapted form of the linear interpolation of the velocities without constraints obtained from expression (20a)

$$\left[\dot{\mathbf{U}}^{\mathrm{A}}_{j-1_{\mathrm{sl}}}\right] = \frac{1}{m}\left[\!\left[\dot{\mathbf{U}}^{\mathrm{A}}_{0_{\mathrm{sl}}}\right]\!\right] \tag{36}$$

We first separate the velocities without constraints from the velocities with constraints:

$$\begin{aligned} E_{\text{interface}} = {} & \frac{1}{m\Delta t}\left[\!\left[\dot{\mathbf{U}}^{\mathrm{A}}_{0_{\mathrm{al}}}\right]\!\right]^{\mathrm{T}}\mathbf{C}^{\mathrm{A}^{\mathrm{T}}}\left[\!\left[\boldsymbol{\Lambda}_0\right]\!\right] + \sum_{j=1}^{m}\frac{1}{\Delta t}\left[\dot{\mathbf{U}}^{\mathrm{B}}_{j-1_{\mathrm{al}}}\right]^{\mathrm{T}}\mathbf{C}^{\mathrm{B}^{\mathrm{T}}}\left[\boldsymbol{\Lambda}_{j-1}\right] \\ & + \frac{1}{m\Delta t}\left[\!\left[\dot{\mathbf{U}}^{\mathrm{A}}_{0_{\mathrm{sl}}}\right]\!\right]^{\mathrm{T}}\mathbf{C}^{\mathrm{A}^{\mathrm{T}}}\left[\!\left[\boldsymbol{\Lambda}_0\right]\!\right] + \sum_{j=1}^{m}\frac{1}{\Delta t}\left[\dot{\mathbf{U}}^{\mathrm{B}}_{j-1_{\mathrm{sl}}}\right]^{\mathrm{T}}\mathbf{C}^{\mathrm{B}^{\mathrm{T}}}\left[\boldsymbol{\Lambda}_{j-1}\right] \end{aligned} \tag{37}$$

Then, we can modify the terms without constraints using expression (32) applied to the Lagrange multipliers together with expression (36)

$$\begin{aligned} E_{\text{interface}} = {} & \frac{1}{m\Delta t}\left[\!\left[\dot{\mathbf{U}}^{\mathrm{A}}_{0_{\mathrm{al}}}\right]\!\right]^{\mathrm{T}}\mathbf{C}^{\mathrm{A}^{\mathrm{T}}}\left[\!\left[\boldsymbol{\Lambda}_0\right]\!\right] + \sum_{j=1}^{m}\frac{1}{\Delta t}\left[\dot{\mathbf{U}}^{\mathrm{B}}_{j-1_{\mathrm{al}}}\right]^{\mathrm{T}}\mathbf{C}^{\mathrm{B}^{\mathrm{T}}}\left[\boldsymbol{\Lambda}_{j-1}\right] \\ & + \sum_{j=1}^{m}\frac{1}{\Delta t}\left(\mathbf{C}^{\mathrm{A}}\left[\dot{\mathbf{U}}^{\mathrm{A}}_{j-1_{\mathrm{sl}}}\right] + \mathbf{C}^{\mathrm{B}}\left[\dot{\mathbf{U}}^{\mathrm{B}}_{j-1_{\mathrm{sl}}}\right]\right)^{\mathrm{T}}\left[\boldsymbol{\Lambda}_{j-1}\right] \end{aligned} \tag{38}$$

The continuity of velocities (10) allows us to express the unconstrained terms as functions of the constrained terms

$$\begin{aligned} E_{\text{interface}} = {} & \frac{1}{m\Delta t}\left[\!\left[\dot{\mathbf{U}}^{\mathrm{A}}_{0_{\mathrm{al}}}\right]\!\right]^{\mathrm{T}}\mathbf{C}^{\mathrm{A}^{\mathrm{T}}}\left[\!\left[\boldsymbol{\Lambda}_0\right]\!\right] + \sum_{j=1}^{m}\frac{1}{\Delta t}\left[\dot{\mathbf{U}}^{\mathrm{B}}_{j-1_{\mathrm{al}}}\right]^{\mathrm{T}}\mathbf{C}^{\mathrm{B}^{\mathrm{T}}}\left[\boldsymbol{\Lambda}_{j-1}\right] \\ & - \sum_{j=1}^{m}\frac{1}{\Delta t}\left(\mathbf{C}^{\mathrm{A}}\left[\dot{\mathbf{U}}^{\mathrm{A}}_{j-1_{\mathrm{al}}}\right] + \mathbf{C}^{\mathrm{B}}\left[\dot{\mathbf{U}}^{\mathrm{B}}_{j-1_{\mathrm{al}}}\right]\right)^{\mathrm{T}}\left[\boldsymbol{\Lambda}_{j-1}\right] \end{aligned} \tag{39}$$

Thus, we obtain

$$E_{\text{interface}} = \frac{1}{m\Delta t}\left[\!\left[\dot{\mathbf{U}}^{\mathrm{A}}_{0_{\mathrm{al}}}\right]\!\right]^{\mathrm{T}}\mathbf{C}^{\mathrm{A}^{\mathrm{T}}}\left[\!\left[\boldsymbol{\Lambda}_0\right]\!\right] - \sum_{j=1}^{m}\frac{1}{\Delta t}\left[\dot{\mathbf{U}}^{\mathrm{A}}_{j-1_{\mathrm{al}}}\right]^{\mathrm{T}}\mathbf{C}^{\mathrm{A}^{\mathrm{T}}}\left[\boldsymbol{\Lambda}_{j-1}\right] \tag{40}$$

Furthermore, expression (22) yields

$$\mathbf{C}^{\mathrm{A}^{\mathrm{T}}}\boldsymbol{\Lambda}_j = \frac{1}{\alpha_{\mathrm{A}}}\tilde{\mathbf{M}}^{\mathrm{A}}\dot{\mathbf{U}}^{\mathrm{A}}_{j_{\mathrm{al}}} \tag{41}$$

i.e.

$$E_{\text{interface}} = \frac{1}{\mathrm{A}}\left(\frac{\left[\!\left[\dot{\mathbf{U}}^{\mathrm{A}}_{0_{\mathrm{al}}}\right]\!\right]^{\mathrm{T}}}{m\Delta t}\tilde{\mathbf{M}}^{\mathrm{A}}\frac{\left[\!\left[\dot{\mathbf{U}}^{\mathrm{A}}_{0_{\mathrm{al}}}\right]\!\right]}{m\Delta t} - \frac{1}{m}\sum_{j=1}^{m}\frac{\left[\dot{\mathbf{U}}^{\mathrm{A}}_{j-1_{\mathrm{al}}}\right]^{\mathrm{T}}}{\Delta t}\tilde{\mathbf{M}}^{\mathrm{A}}\frac{\left[\dot{\mathbf{U}}^{\mathrm{A}}_{j-1_{\mathrm{al}}}\right]}{\Delta t}\right) \tag{42}$$

In order to conclude, concerning the stability of this algorithm, we study the sign of expression (42). For this purpose, we will study a scalar expression equivalent to matrix expression (42)

$$\tilde{E}^{m}_{\text{interface}} = (\alpha_{n+m} - \alpha_n)^2 - m \sum_{j=1}^{m} (\alpha_{n+j} - \alpha_{n+j-1})^2 \tag{43}$$

When $m = 2$:

$$\tilde{E}^{2}_{\text{interface}} = (\alpha_{n+2} - \alpha_n)^2 - 2 \sum_{j=1}^{2} (\alpha_{n+j} - \alpha_{n+j-1})^2 \tag{44}$$

we obtain

$$\tilde{E}^{2}_{\text{interface}} = -((\alpha_{n+2} - \alpha_{n+1}) - (\alpha_{n+1} - \alpha_n))^2 \tag{45}$$

When $m = 3$:

$$\tilde{E}^{3}_{\text{interface}} = (\alpha_{n+3} - \alpha_n)^2 - 3 \sum_{j=1}^{3} (\alpha_{n+j} - \alpha_{n+j-1})^2 \tag{46}$$

we obtain

$$\begin{aligned} \tilde{E}^{3}_{\text{interface}} = &-((\alpha_{n+3} - \alpha_{n+2}) - (\alpha_{n+2} - \alpha_{n+1}))^2 - ((\alpha_{n+3} - \alpha_{n+2}) - (\alpha_{n+1} - \alpha_n))^2 \\ &- ((\alpha_{n+2} - \alpha_{n+1}) - (\alpha_{n+1} - \alpha_n))^2 \end{aligned} \tag{47}$$

Finally, one can show that for any non-zero integer m we have

$$\begin{aligned} \tilde{E}^{m}_{\text{interface}} = &-((\alpha_{n+m} - \alpha_{n+m-1}) - (\alpha_{n+m-1} - \alpha_{n+m-2}))^2 - ((\alpha_{n+m} - \alpha_{n+m-1}) - (\alpha_{n+m-2} - \alpha_{n+m-3}))^2 \\ &- \cdots - ((\alpha_{n+m} - \alpha_{n+m-1}) - (\alpha_{n+1} - \alpha_n))^2 - ((\alpha_{n+m-1} - \alpha_{n+m-2}) - (\alpha_{n+m-2} - \alpha_{n+m-3}))^2 \\ &- \cdots - ((\alpha_{n+m-1} - \alpha_{n+m-2}) - (\alpha_{n+1} - \alpha_n))^2 \\ &\vdots \quad \vdots \\ &- ((\alpha_{n+2} - \alpha_{n+1}) - (\alpha_{n+1} - \alpha_n))^2 \end{aligned} \tag{48}$$

where expression (48) has $m(m-1)/2$ terms.

Therefore, we conclude that expression (42) is a sum of negative squares defined by

$$\begin{aligned} E_{\text{interface}} = -\frac{1}{\text{A}} \sum_{i=1}^{m-1} \sum_{j=i}^{m-1} \Bigg(&\frac{\left(\left(\dot{\mathbf{U}}^{\text{A}}_{m-i+1_{\text{al}}} - \dot{\mathbf{U}}^{\text{A}}_{m-i_{\text{al}}}\right) - \left(\dot{\mathbf{U}}^{\text{A}}_{m-j_{\text{al}}} - \dot{\mathbf{U}}^{\text{A}}_{m-j-1_{\text{al}}}\right)\right)^{\text{T}}}{2\Delta t} \tilde{\mathbf{M}}^{\text{A}} \\ &\times \frac{\left(\left(\dot{\mathbf{U}}^{\text{A}}_{m-i+1_{\text{al}}} - \dot{\mathbf{U}}^{\text{A}}_{m-i_{\text{al}}}\right) - \left(\dot{\mathbf{U}}^{\text{A}}_{m-j_{\text{al}}} - \dot{\mathbf{U}}^{\text{A}}_{m-j-1_{\text{al}}}\right)\right)}{2\Delta t} \Bigg) \leqslant 0 \end{aligned} \tag{49}$$

Theorem 1. If, for each subdomain, $\gamma_k \geqslant \frac{1}{2}$, then matrix $\mathbf{A}$ is positive definite, and if $\tilde{\mathbf{M}}$ is positive definite, then $\ddot{\mathbf{U}}$ and $\dot{\mathbf{U}}$ are bounded (proof identical to that proposed in Reference [8]).

(50)

The advantage of this formulation and this theorem is that one can study the stability of the Newmark numeric scheme directly from $\mathbf{A}$ because, on the one hand, $\tilde{\mathbf{M}}$ is positive definite by definition and, on the other hand, if we use the eigenmodes to diagonalize matrix $\mathbf{A}$, we get a second-degree inequality in Δt expressing that the latter is positive definite

$$1 + \left(\quad - \frac{}{2} \right) (\omega \Delta t)^2 \geqslant 0 \tag{51}$$

where ω are the eigenvalues of matrix $\mathbf{A}$. Thus, we end up with the classical stability conditions of Newmark's numeric scheme [46]:

$$\tfrac{1}{2} \leqslant \gamma \leqslant 2\beta, \quad \text{unconditionally stable method} \tag{52}$$

$$\tfrac{1}{2} \leqslant \quad \text{and} \quad 2\beta \leqslant \gamma, \quad \text{conditionally stable method,} \quad \Delta t \leqslant \frac{1}{\omega_{\max} \sqrt{\gamma/2 - }} \tag{53}$$

with the definition $\omega_{\max} = \sup\{\omega\}$.

According to Equation (24), if theorem 1 is verified and if $\mathbf{H}$ is invertible, then the Lagrange multipliers are bounded. Furthermore, if $\mathbf{K}^{-1}$ exists, then from (8) $\mathbf{U}_{n+1}$ is bounded in each subdomain. The numerical damping term (see (29)) also allows us to conclude that, if $\gamma = \frac{1}{2}$ in a subdomain, the associated numeric scheme does not dissipate energy (second-order scheme); conversely, if $\gamma \geqslant \frac{1}{2}$, the scheme dissipates energy (first-order scheme). This is in complete agreement with the definition of the algorithmic damping rate of the Newmark family of numeric schemes [47]:

$$\xi_{\text{num}} = \pi \left(\quad - \frac{1}{2} \right) \frac{\Delta t}{T} + O\left(\left(\frac{\Delta t}{T} \right)^2 \right) \tag{54}$$

Remarks. It is possible to take the mechanical damping into account. In such a case, Equation (29) contains an additional term related to the mechanical damping and different from the numerical damping term. In this case, the same method leads to the stability equations for Newmark schemes with mechanical damping [46].

The stability of the global problem depends on the stability conditions of the Newmark numeric schemes considered in each subdomain. Thus, the convergence rate of the Newmark numeric schemes is defined by expression (54). Consequently, the global convergence rate is defined as the minimum of the convergence rates for each subdomain. Thus, if, for example, we use parameters $\gamma_{\text{B}} = \frac{1}{2}$, $\beta_{\text{B}} = 0$, $\gamma_{\text{A}} = \frac{1}{2}$, $\beta_{\text{A}} = \frac{1}{4}$ to couple explicit and implicit numeric schemes each with a second-order convergence rate, and if the term associated with the interfacial energy is zero, then the scheme is globally of the second order.

The algorithm studied is stable, but can present numerical dissipation at the interface (see (49)). Expression (49) shows that if the velocity of subdomain A is constant on the coarse time scale, then the numerical dissipation equals zero; otherwise, energy dissipates at the interface. In other terms, when the displacement of subdomain A is not linear with time, the smaller the local radius of curvature, the higher the numerical dissipation.

Finally, with this approach, the coupling of different numeric schemes of the Newmark family has no influence on the stability of these schemes. Thus, implicit subdomains remain unconditionally stable and explicit subdomains remain conditionally stable with the same

stability limits. One can conclude from this result that the ratio of the time step in subdomain A to the time step in subdomain B has no direct effect on the stability of the algorithm; however, this parameter conditions, the quality of the interpolation of the kinematic quantities of subdomain A, which the method's numerical damping depends on directly.

3. STUDY OF THE NON-LINEAR CASE

3.1. Treatment of non-linearities

3.1.1. Material non-linearities. Let us assume that the constitutive law associated with some subdomains is non-linear, for example elastic–plastic with kinematic hardening. For certain problems where the non-linearities are localized within a structure, they can be associated with an explicit subdomain with a non-linear constitutive law and a fine time scale defined by the critical time step, whereas implicit subdomains with a linear constitutive law and a coarse time scale are used in the rest of the structure. In this case, the algorithm in Section 2 remains the same, but the unconstrained problem of the explicit subdomain becomes

$$\mathbf{M}^{\mathrm{B}}\ddot{\mathbf{U}}^{\mathrm{B}}_{j_{\mathrm{free}}} = \mathbf{F}^{\mathrm{B}}_{\mathrm{ext}_j} - \mathbf{F}^{\mathrm{B}}_{\mathrm{int}_j}\left({}^{\mathrm{p}}\mathbf{U}^{\mathrm{B}}_{j-1}\right) \tag{55}$$

with

$$\mathbf{M}^{\mathrm{B}}\text{: diagonal mass matrix} \tag{56}$$

Similarly, the algorithm can be immediately generalized to the explicit non-linear/explicit non-linear case with different time steps in the two subdomains. In this case, the unconstrained equations associated with each subdomain are of form (55). One can also note that if the two subdomains are explicit, whether linear or non-linear, the interface operator (25) is diagonal. We are now concerned with the implicit non-linear/explicit non-linear case where the fine time scale is associated with the explicit domain (designated by E), and the coarse time scale with the implicit subdomain (designated by I). In the following, we keep the general formalism of the Newmark schemes, yet with the condition

$$\beta_{\mathrm{E}} = 0 \tag{57}$$

In this case, equilibrium Equations (8) and (9) become

$$\mathbf{M}^{\mathrm{I}}\ddot{\mathbf{U}}^{\mathrm{I}}_{m} + \mathbf{F}^{\mathrm{I}}_{\mathrm{int}}\left(\mathbf{U}^{\mathrm{I}}_{m}\right) = \mathbf{F}^{\mathrm{I}}_{\mathrm{ext}_m} + \mathbf{C}^{\mathrm{I}^{\mathrm{T}}}\boldsymbol{\Lambda}_m \tag{58}$$

$$\mathbf{M}^{\mathrm{E}}\ddot{\mathbf{U}}^{\mathrm{E}}_{j} + \mathbf{F}^{\mathrm{E}}_{\mathrm{int}_j}\left({}^{\mathrm{p}}\mathbf{U}^{\mathrm{E}}_{j-1}\right) = \mathbf{F}^{\mathrm{E}}_{\mathrm{ext}_j} + \mathbf{C}^{\mathrm{E}^{\mathrm{T}}}\boldsymbol{\Lambda}_j \tag{59}$$

Concerning the calculation of the internal forces of the explicit subdomain, they can simply be calculated using the plastically admissible stresses. To calculate the internal forces of the implicit subdomain, we perform, on the one hand, a plastic projection of the stresses and, on the other hand, iterations on the equilibrium (58) which we call 'external iterations'. The plastic projection uses a radial return method on the threshold [48]. The implementation of external iterations starting from the Newton method requires more care because of the Lagrange multipliers and the two time discretizations [49]. First, the residuals $\mathbf{R}^{(i-1)}_{m}$ at the

equilibrium for iteration $(i-1)$ and the linearized expression $\mathbf{R}_m^{*(i)}$ at iteration (i) are defined

$$\mathbf{R}_m^{(i-1)} = \mathbf{F}_{\text{ext}_m}^{\text{I}} + \mathbf{C}^{\text{I}^{\text{T}}} \boldsymbol{\Lambda}_m^{(i-1)} - \mathbf{M}^{\text{I}} \left(\frac{\mathbf{U}_m^{\text{I}^{(i-1)}} - {}^{\text{p}}\mathbf{U}_n^{\text{I}}}{\beta_1 (m\Delta t)^2} \right) - \mathbf{F}_{\text{int}_m}^{\text{I}^{(i-1)}} \tag{60}$$

$$\mathbf{R}_m^{*(i)} = \mathbf{R}_m^{(i-1)} + \mathbf{A}_1 \Delta\Delta \mathbf{U}_m^{\text{I}^{(i)}} + \mathbf{A}_2 \Delta\Delta \boldsymbol{\Lambda}_m^{\text{I}^{(i)}} \tag{61}$$

with

$$\mathbf{A}_1 \equiv \left[\frac{\partial \mathbf{R}}{\partial \mathbf{U}} \right]_{\mathbf{U}_m^{\text{I}^{(i-1)}}} = -\left(\mathbf{K}_t^{\text{I}} + \frac{1}{\beta_1 (m\Delta t)^2} \mathbf{M}^{\text{I}} \right) \quad \text{and} \quad \mathbf{A}_2 \equiv \left[\frac{\partial \mathbf{R}}{\partial \boldsymbol{\Lambda}} \right]_{\boldsymbol{\Lambda}_m^{\text{I}^{(i-1)}}} = \mathbf{C}^{\text{I}^{\text{T}}} \tag{62}$$

In the first stage, we assume that matrix $\mathbf{K}_t^{\text{I}}$ remains constant during the equilibrium iterations. Then, we apply the Newton–Raphson method with the assumption that the linearized equation (61) is verified, i.e. the linearized residual (61) equals zero. This leads to the equilibrium equation on the coarse time scale

$$\tilde{\mathbf{K}}_t^{\text{I}} \Delta\Delta \mathbf{U}_m^{\text{I}^{(i)}} = \mathbf{R}_m^{(i-1)} + \mathbf{C}^{\text{I}^{\text{T}}} \Delta\Delta \boldsymbol{\Lambda}_m^{(i)} \tag{63}$$

with

$$\tilde{\mathbf{K}}_t^{\text{I}} = \mathbf{K}_t^{\text{I}} + \frac{1}{\beta_1 (m\Delta t)^2} \mathbf{M}^{\text{I}} \tag{64}$$

$$\Delta \mathbf{U}_m^{\text{I}} = \sum_{i=1}^{r} \Delta\Delta \mathbf{U}_m^{\text{I}^{(i)}}, \quad \Delta \boldsymbol{\Lambda}_m = \sum_{i=1}^{r} \Delta\Delta \boldsymbol{\Lambda}_m^{(i)} \tag{65}$$

$$\mathbf{U}_m^{\text{I}} = \mathbf{U}_0^{\text{I}} + \Delta \mathbf{U}_m^{\text{I}}, \quad \boldsymbol{\Lambda}_m = \boldsymbol{\Lambda}_0 + \Delta \boldsymbol{\Lambda}_m \tag{66}$$

and r the index at the convergence. We will show that we can perform the external iterations on the coarse time scale only. For this purpose, let us show that the increment in the Lagrange multipliers can be calculated from the unconstrained problem in the coarse time scale. Let us write the linearized equations for the continuity of velocities at the interface (10), the transition operators from the coarse to the fine time scale (12) (13) and the equilibrium equation on the fine time scale (59) which, added to Equation (63), determine the increment in the multipliers

$$\mathbf{M}^{\text{E}} \Delta\Delta \ddot{\mathbf{U}}_j^{\text{E}^{(i)}} = \mathbf{C}^{\text{E}^{\text{T}}} \Delta\Delta \boldsymbol{\Lambda}_j^{(i)} \tag{67}$$

$$\mathbf{C}^{\text{I}} \Delta\Delta \dot{\mathbf{U}}_j^{\text{I}^{(i)}} + \mathbf{C}^{\text{E}} \Delta\Delta \dot{\mathbf{U}}_j^{\text{E}^{(i)}} = 0 \tag{68}$$

$$\mathbf{C}^{\text{I}} \Delta\Delta \dot{\mathbf{U}}_j^{\text{I}^{(i)}} = \frac{j}{m} \mathbf{C}^{\text{I}} \Delta\Delta \dot{\mathbf{U}}_m^{\text{I}^{(i)}} \tag{69}$$

$$\Delta\Delta \boldsymbol{\Lambda}_j^{(i)} = \frac{j}{m} \Delta\Delta \boldsymbol{\Lambda}_j^{(i)} \tag{70}$$

Moreover, we have the linearized Newmark equations

$$\Delta\Delta\dot{\mathbf{U}}_m^{\mathrm{I}^{(i)}} = \gamma_{\mathrm{I}}(m\Delta t)\Delta\Delta\ddot{\mathbf{U}}_m^{\mathrm{I}^{(i)}} \tag{71}$$

$$\Delta\Delta\mathbf{U}_m^{\mathrm{I}^{(i)}} = \beta_{\mathrm{I}}(m\Delta t)^2\Delta\Delta\ddot{\mathbf{U}}_m^{\mathrm{I}^{(i)}} \tag{72}$$

$$\Delta\Delta\dot{\mathbf{U}}_j^{\mathrm{E}^{(i)}} = \gamma_{\mathrm{E}}\Delta t\Delta\Delta\ddot{\mathbf{U}}_j^{\mathrm{E}^{(i)}} \tag{73}$$

Then, we can write the problem in matrix form

$$\begin{pmatrix} \gamma_{\mathrm{I}}(j\Delta t)\tilde{\mathbf{M}}_t^{\mathrm{I}} & 0 & -{}_{\mathrm{I}}(m\Delta t)\mathbf{C}^{\mathrm{I}^{\mathrm{T}}} \\ 0 & \gamma_{\mathrm{E}}\Delta t\mathbf{M}^{\mathrm{E}} & -{}_{\mathrm{E}}\Delta t\mathbf{C}^{\mathrm{E}^{\mathrm{T}}} \\ -{}_{\mathrm{I}}(j\Delta t)\mathbf{C}^{\mathrm{I}} & -\gamma_{\mathrm{E}}\Delta t\mathbf{C}^{\mathrm{E}} & 0 \end{pmatrix} \begin{pmatrix} \Delta\Delta\ddot{\mathbf{U}}_m^{\mathrm{I}^{(i)}} \\ \Delta\Delta\ddot{\mathbf{U}}_j^{\mathrm{E}^{(i)}} \\ \Delta\Delta\boldsymbol{\Lambda}_j^{(i)} \end{pmatrix} = \begin{pmatrix} {}_{\mathrm{I}}(j\Delta t)\mathbf{R}_m^{(i-1)} \\ 0 \\ 0 \end{pmatrix} \tag{74}$$

As in the linear case, we can decompose the global problem into the first, unconstrained problem and the second, constrained one. The unconstrained equilibrium is

$$\begin{pmatrix} \tilde{\mathbf{M}}_t^{\mathrm{I}} & 0 & 0 \\ 0 & \mathbf{M}^{\mathrm{E}} & 0 \\ 0 & 0 & 0 \end{pmatrix} \begin{pmatrix} \Delta\Delta\ddot{\mathbf{U}}_{m_{\mathrm{free}}}^{\mathrm{I}^{(i)}} \\ \Delta\Delta\ddot{\mathbf{U}}_{j_{\mathrm{free}}}^{\mathrm{E}^{(i)}} \\ 0 \end{pmatrix} = \begin{pmatrix} \mathbf{R}_m^{(i-1)} \\ 0 \\ 0 \end{pmatrix} \tag{75}$$

From the second line of Equation (75), we get

$$\Delta\Delta\ddot{\mathbf{U}}_{j_{\mathrm{free}}}^{\mathrm{E}^{(i)}} = 0 \tag{76}$$

The equations of the constrained problem are given by

$$\begin{pmatrix} \gamma_{\mathrm{I}}(j\Delta t)\tilde{\mathbf{M}}_t^{\mathrm{I}} & 0 & -{}_{\mathrm{I}}(m\Delta t)\mathbf{C}^{\mathrm{I}^{\mathrm{T}}} \\ 0 & \gamma_{\mathrm{E}}\Delta t\mathbf{M}^{\mathrm{E}} & -{}_{\mathrm{E}}\Delta t\mathbf{C}^{\mathrm{E}^{\mathrm{T}}} \\ 0 & 0 & \mathbf{H}_t \end{pmatrix} \begin{pmatrix} \Delta\Delta\ddot{\mathbf{U}}_{m_{\mathrm{link}}}^{\mathrm{I}^{(i)}} \\ \Delta\Delta\ddot{\mathbf{U}}_{j_{\mathrm{link}}}^{\mathrm{E}^{(i)}} \\ \Delta\Delta\boldsymbol{\Lambda}_{\mathrm{j}}^{(i)} \end{pmatrix} = \begin{pmatrix} {}_{\mathrm{I}}(j\Delta t)\mathbf{R}_m^{(i-1)} \\ 0 \\ -(\mathbf{C}^{\mathrm{I}}\Delta\Delta\dot{\mathbf{U}}_{j_{\mathrm{free}}}^{\mathrm{I}^{(i)}} + \mathbf{C}^{\mathrm{E}}\Delta\Delta\dot{\mathbf{U}}_{j_{\mathrm{free}}}^{\mathrm{E}^{(i)}}) \end{pmatrix} \tag{77}$$

where $\mathbf{H}_t$ is the condensation operator associated with the constant matrix $\mathbf{K}_t^{\mathrm{I}}$.

From Equations (73), (76) and (77), we see that the increment in Lagrange multipliers depends only on the increment in implicit unconstrained velocity

$$\mathbf{H}_t\Delta\Delta\boldsymbol{\Lambda}_j^{(i)} = -\mathbf{C}^{\mathrm{I}}\Delta\Delta\dot{\mathbf{U}}_{j_{\mathrm{free}}}^{\mathrm{I}^{(i)}} \tag{78}$$

This shows that the corrections applied at each iteration on the condensed problem at the interfaces depend only on the coarse time scale, because the quantity $\Delta\Delta\dot{\mathbf{U}}_{j_{\mathrm{free}}}^{\mathrm{I}^{(i)}}$ is interpolated from the unconstrained velocities of the coarse time scale. Thus, the external iterations on the equilibrium of implicit subdomain I can be performed directly on the coarse time scale as opposed to the fine time scale.

① loop on time steps of the coarse scale
②external iterations
solve the "unconstrained" problem for subdomain I
③loop on the m time steps of the fine scale
calculate the internal forces of subdomain E
solve the "unconstrained" problem for the subdomain
change scale at the edge of subdomain I
calculate the Lagrange multipliers
solve the "constrained" problem for subdomain E
calculate the kinematic quantities of subdomain E
if $j=m$, then end loop
solve the "constrained" problem for subdomain I
calculate the kinematic quantities of subdomain I
calculate the internal forces of subdomain I
calculate the residuals
if termination criterion then end external iterations
end loop on the coarse time scale

Figure 5. Flow-chart of the new mixed- and multi-time step method in the non-linear case.

3.1.2. Geometric non-linearities The previous algorithm can also be generalized to the case of large displacements. It suffices to try to write the equilibrium of the Cauchy stresses on the deformed geometry, and, therefore, reactualize the configuration when calculating the internal forces, both on the implicit and explicit subdomains. Thus, the calculation of the internal forces proceeds as follows: first, the internal iterations yield a stress increment which is used to calculate the associated Piola–Kirchoff stresses. Finally, these are used to express the internal forces and the corresponding residuals

$$\mathbf{F}^{\mathrm{I}^{(i)}}_{\mathrm{int}_m} = \int_{\Omega^{\mathrm{I}^{(i)}}_m} \mathbf{B}^{\mathrm{I}^{(i)\mathrm{T}}}_m \sigma^{\mathrm{I}^{(i)}}_m \, \mathrm{d}\Omega \tag{79}$$

$$\mathbf{R}^{\mathrm{I}^{(i)}}_m = \frac{1}{\beta(m\Delta t)^2}\mathbf{M}^{\mathrm{I}}\left(\mathbf{U}^{\mathrm{I}^{(i)}}_m - {}^{\mathrm{p}}\mathbf{U}^1_0\right) + \mathbf{F}^{\mathrm{I}^{(i)}}_{\mathrm{int}_m} - \mathbf{F}^{\mathrm{I}^{(i)}}_{\mathrm{ext}_m} \tag{80}$$

$$\mathbf{F}^{\mathrm{E}}_{\mathrm{int}_m} = \int_{\substack{\mathrm{E}\\ m}} \mathbf{B}^{\mathrm{E}^{\mathrm{T}}}_m \sigma^{\mathrm{E}}_m \, \mathrm{d}\Omega \tag{81}$$

where σ and $\mathbf{F}^{\mathrm{I}^{(i)}}_{\mathrm{ext}_m}$ designate, respectively, the Cauchy stress and the external forces on the deformed geometry. Once these calculations have been performed, one must go back to the previous configuration if external iterations on the implicit subdomain are needed.

3.2. Implementation—algorithm

This result can be expressed in the form of an algorithm (Figure 5):

This algorithm is presented in the case of two subdomains with two different time scales. One can generalize the method to the case of s subdomains with s different time scales. One uses a double termination criterion

$$\frac{\|\mathbf{R}^{\mathrm{I}^{(i)}}_m\|}{\|\mathbf{F}^{\mathrm{I}^{(i)}}_{\mathrm{int}_m}\|} \leqslant \varepsilon_1 \quad \text{and} \quad \|\Delta\Delta\mathbf{U}^{\mathrm{I}^{(i)}}_m\| \leqslant \varepsilon_2 \tag{82}$$

This algorithm must also be adjusted, for example, depending on the type of finite elements considered: thus, in the case of structures modeled with shell elements, one must distinguish between membrane forces and bending moments in the calculation of the residuals [50].

3.3. Stability

Concerning the stability and global convergence of the algorithm in the non-linear case, we can make the following remarks: the concept of stability used in Section 2.2 defines only necessary conditions for stability in the non-linear case [13]. (In the linear case, they are necessary and sufficient.) However, we can make the following observations: the condition on the explicit time step is sufficient; if the non-linear response is carefully discretized by the chosen time step, the stability conditions are sufficient for the implicit subdomains; if the non-linear response is not discretized with sufficient precision, cumulative roundoff errors may dominate and degrade, or even amplify slightly, the numerical solution. In the geometric non-linear case, the time step Δt often varies because the size of the elements changes at each time step. The same type of approach can be followed with a variable time step. The end result is that the term associated with the energy dissipated at the interface is bounded by (see (49))

$$-\frac{1}{\gamma_{\mathrm{A}}\Delta t_{\min}^2}\sum_{i=1}^{m-1}\sum_{j=i}^{m-1}\left(\frac{\left(\left(\dot{\mathbf{U}}^{\mathrm{A}}_{m-i+1_{\mathrm{al}}}-\dot{\mathbf{U}}^{\mathrm{A}}_{m-i_{\mathrm{al}}}\right)-\left(\dot{\mathbf{U}}^{\mathrm{A}}_{m-j_{\mathrm{al}}}-\dot{\mathbf{U}}^{\mathrm{A}}_{m-j-1_{\mathrm{al}}}\right)\right)^{\mathrm{T}}}{2}\tilde{\mathbf{M}}^{\mathrm{A}}\right.$$
$$\left.\times\frac{\left(\left(\dot{\mathbf{U}}^{\mathrm{A}}_{m-i+1_{\mathrm{al}}}-\dot{\mathbf{U}}^{\mathrm{A}}_{m-i_{\mathrm{al}}}\right)-\left(\dot{\mathbf{U}}^{\mathrm{A}}_{m-j_{\mathrm{al}}}-\dot{\mathbf{U}}^{\mathrm{A}}_{m-j-1_{\mathrm{al}}}\right)\right)}{2}\right)\leqslant E_{\mathrm{interface}} \tag{83}$$

$$E_{\mathrm{interface}}\leqslant-\frac{1}{\gamma_{\mathrm{A}}\Delta t_{\max}^2}\sum_{i=1}^{m-1}\sum_{j=i}^{m-1}\left(\frac{\left(\left(\dot{\mathbf{U}}^{\mathrm{A}}_{m-i+1_{\mathrm{al}}}-\dot{\mathbf{U}}^{\mathrm{A}}_{m-i_{\mathrm{al}}}\right)-\left(\dot{\mathbf{U}}^{\mathrm{A}}_{m-j_{\mathrm{al}}}-\dot{\mathbf{U}}^{\mathrm{A}}_{m-j-1_{\mathrm{al}}}\right)\right)^{\mathrm{T}}}{2}\tilde{\mathbf{M}}^{\mathrm{A}}\right.$$
$$\left.\times\frac{\left(\left(\dot{\mathbf{U}}^{\mathrm{A}}_{m-i+1_{\mathrm{al}}}-\dot{\mathbf{U}}^{\mathrm{A}}_{m-i_{\mathrm{al}}}\right)-\left(\dot{\mathbf{U}}^{\mathrm{A}}_{m-j_{\mathrm{al}}}-\dot{\mathbf{U}}^{\mathrm{A}}_{m-j-1_{\mathrm{al}}}\right)\right)}{2}\right)\leqslant 0 \tag{84}$$

where $\Delta t_{\min}$ and $\Delta t_{\max}$ correspond, respectively, to the smallest and the largest time step on the interval ΔT. Consequently, the method chosen to couple the subdomains does not affect the stability of the numeric scheme of each subdomain. The known results for a single subdomain in non-linear dynamics are thus applicable. The dissipation at the interface may, however, affect the convergence rate of the calculation schemes.

4. EXAMPLES

The examples considered below were calculated on the CASTEM 2000 programme developed at the *Commissariat à l'Energie Atomique* [51]. Subsequently, we will assume the explicit numeric scheme to be the central difference scheme $\gamma_{\mathrm{E}}=\frac{1}{2}$ and $\beta_{\mathrm{E}}=0$ and the implicit numeric scheme to be the mean acceleration scheme $\gamma_{\mathrm{I}}=\frac{1}{2}$ and $\beta_{\mathrm{I}}=\frac{1}{4}$.

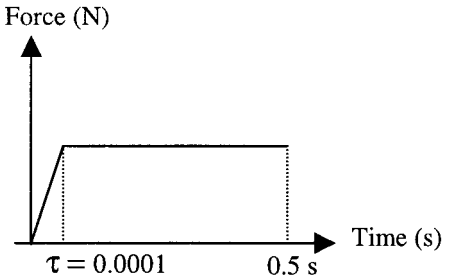

Figure 6. Bending load applied at the end of the beam.

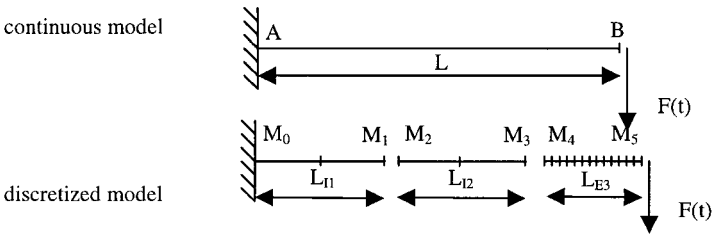

Figure 7. Continuous model and discretized model of the beam.

4.1. Case of a beam in bending

We first consider the case of the fixed/free beam subject to the following load as shown in Figure 6.

This example is treated with a mesh made of three subdomains where the interfaces are reduced to a single node with six degrees of freedom. The objective is to apply to each subdomain an integration scheme which can be explicit or implicit thanks to the unique formalism of Newmark's numeric scheme. The characteristics of the beam are shown in Figure 7.

Characteristics of the subdomains:

$$L_{I_1} = L_{I_2} = \tfrac{15}{32}\,\mathrm{m}$$
$$E_{I_1} = E_{I_2} = 210 \times 10^9\,\mathrm{N\,m^{-2}}$$
$$S_{I_1} = S_{I_2} = 0.01 \times 0.01\,\mathrm{m^2}$$
$$n_{I_1} = n_{I_2} = 10$$
$$\rho_{I_1} = \rho_{I_2} = 7800\,\mathrm{kg\,m^{-3}}$$
$$L_{E_3} = \tfrac{1}{16}\,\mathrm{m}$$
$$E_{E_3} = 210.10^9\,\mathrm{N\,m^{-2}}$$
$$S_{E_3} = 0.01 \times 0.01\mathrm{m^2}$$
$$n_{E_3} = 15$$
$$\rho_{E_3} = 7800\,\mathrm{kg\,m^{-3}}$$

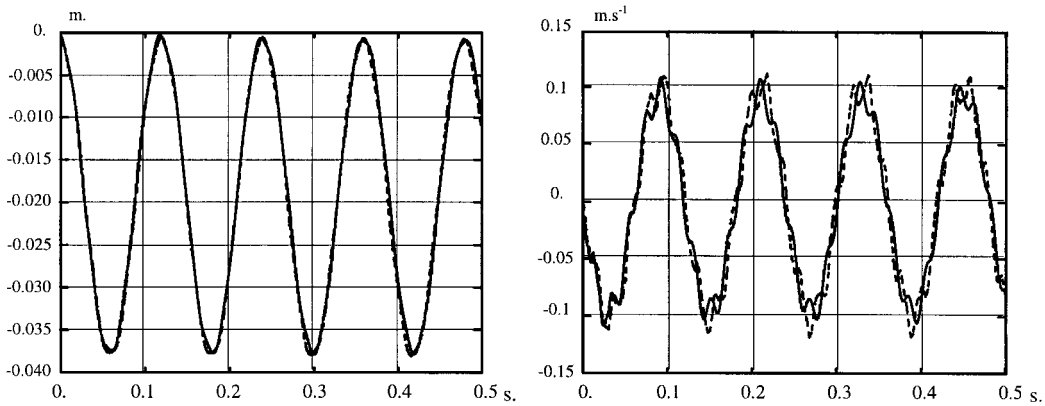

Figure 8. Vertical displacement of the end point and vertical velocity of the end point.

where L designates the length of the subdomain, E its Young's modulus, S its section, n the number of elements of the discretized subdomain and ρ the mass density.

This first example allows us to validate in a one-dimensional case the different configurations presented earlier. The different curves shown below correspond to the displacement and velocity of node M_5. We use as reference subdomain E_3 with the critical time step defined by the Courant condition in the case of the central difference explicit scheme

$$\Delta t_{\text{exp}} = 2.84 \times 10^{-7} \text{ s.}$$

4.2. Analysis of the example with a linear elastic constitutive law ($m = 10\,000$)

We assume small displacements and $\Delta t_{\text{imp}} = m\Delta t_{\text{exp}}$. In addition, we consider that the whole beam is made of a linear elastic, homogeneous, isotropic material. In this case, the maximum bending load is chosen equal to 10 Newtons. In this example, we compare the vertical velocity and displacement of the beam calculated by the method with subcycling to the results obtained with the mean acceleration implicit numeric scheme applied to the structure with no decomposition into subdomains.

Figure 8 represents, respectively, the vertical displacement and velocity of the end point of the beam (continuous line) compared with the reference method (discontinuous line). For this calculation, we chose a ratio of 10 000 between the time steps for the explicit and the implicit parts. The calculation was performed over 0.5 s and requires 1 800 000 explicit time steps. However, the problem has very few degrees of freedom and can be solved in a reasonable amount of time. In order to compare the subcycling method, we calculate an energy balance (see [46]) which reveals that the dissipation at the interface is 1.3 per cent at the end of the calculation (Figure 9). The latter is practically indistinguishable from the abscissa and the total energy of the problem. Thus, this confirms that large time step ratios are acceptable as long as the energy dissipated at the interface between subdomains remains small. One can conclude from these first results that one can envisage large time step ratios between the explicit and implicit schemes with a linear elastic constitutive law assuming small perturbation, without degradation of the displacement and velocity responses.

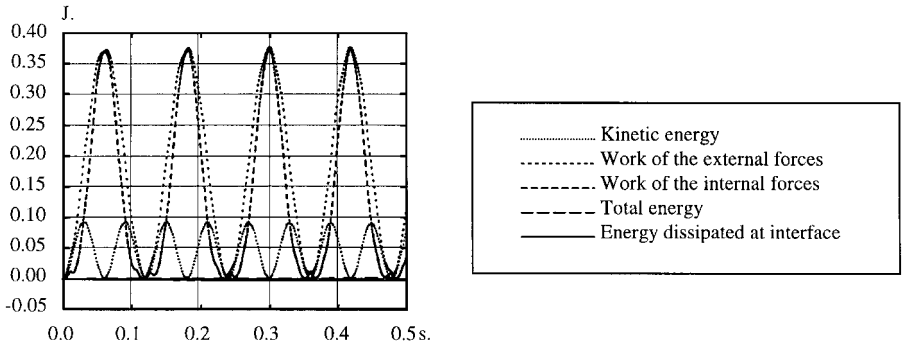

Figure 9. Energy balance.

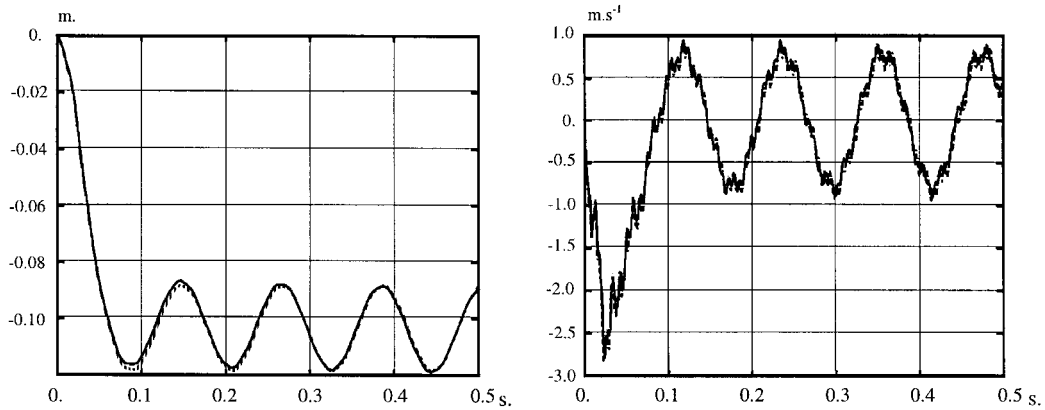

Figure 10. Vertical displacement of the end point and vertical velocity of the end point.

4.3. Analysis of the example with a non-linear constitutive law ($m = 1000$)

Again we assume small perturbations. However, we now consider that the whole beam is made of a homogeneous, isotropic material with an elastic–plastic non-linear constitutive law with strain hardening (yield stress 400 Mpa and tangent modulus equal to 1 per cent of Young's modulus). The maximum bending moment in this case is chosen to be equal to 25 N. We compare the vertical velocity and displacement of the beam calculated by the method with subcycling to the results obtained by a Newton method coupled to the mean acceleration implicit numeric scheme applied to the structure with no decomposition into subdomains.

As in the previous case, we calculate an energy balance of the analysis in order to verify that the energy dissipated at the interfaces is negligible compared to the other energy quantities. The vertical displacement of the end of the beam illustrated on the left-hand curve in Figure 10 reveals a slightly smaller displacement with the subcycling method (continuous line); nevertheless, the comparison is very good. This can be explained by the large time step ratio we considered. The numerical dissipation through the interface between the explicit and implicit subdomains can be seen in Figure 11, but it is very small (0.4 per cent). One

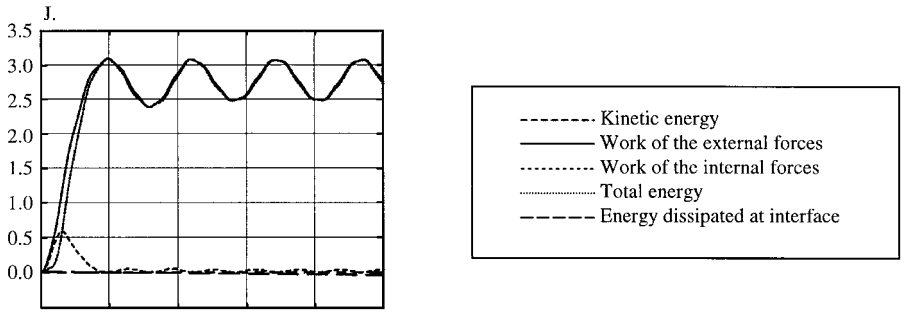

Figure 11. Energy balance.

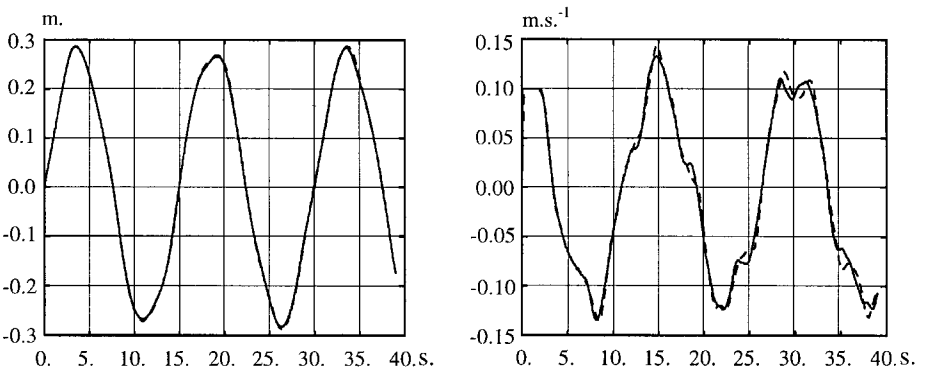

Figure 12. Horizontal displacement of the end point and horizontal velocity of the end point.

can conclude from this second study that one may consider large time step ratios between the explicit and implicit schemes with a elastic–plastic constitutive law and assuming small perturbations, without excessive degradation of the displacement and velocity responses.

4.4. Case of a bar in traction

In this section, we try to compare the method using the validation example proposed in Reference [9]. The problem concerns a fixed-free bar with a length of 540, subjected to an initial horizontal, uniform velocity field equal to 0.1. The bar is decomposed into three subdomains, respectively, explicit, implicit and explicit, with lengths of 180, 300 and 180; furthermore, each subdomain is made of 18, 10 and 18 bar elements, respectively. The area of the section and the density are both equal to 1. In an initial study, the implicit subdomain is defined with a Young's modulus equal to 10^7 and the explicit subdomains with a Young's modulus equal to 10^4. In this case, the critical time step of the explicit subdomains equals 0.1. The calculation is performed with an explicit time step equal to the critical time step and a time step ratio of three between implicit and explicit.

Figure 12 represents, respectively, the horizontal displacement and the velocity of beam's end point. The method with subcycling (continuous line) is compared with the mean acceleration Newmark scheme (discontinuous line). In either case, the time step of the reference

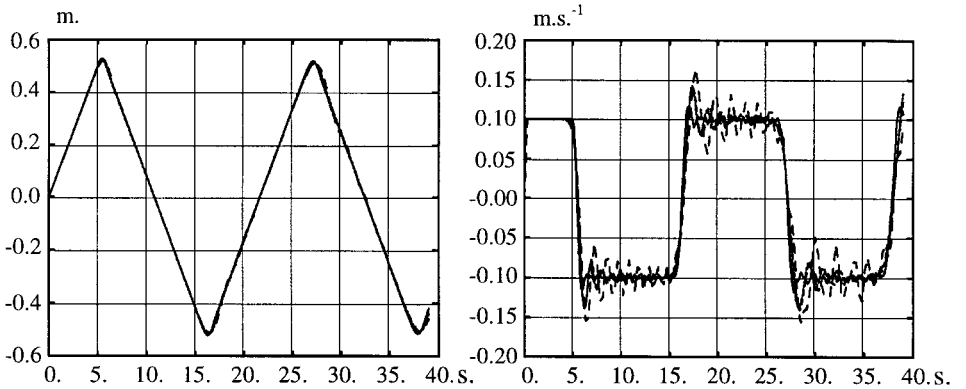

Figure 13. Horizontal displacement of the end point and horizontal velocity of the end point.

implicit method equals the implicit time step of the method with subcycling. The second case study is considered, this time with the same Young's modulus, equal to 10^4, for the three subdomains. The critical time step associated with the elements of the implicit subdomain is 0.3.

Figure 13 also shows the horizontal displacement and velocity of the end point of the beam. The method with subcycling is used in the three cases explicit/explicit (continuous line), implicit/explicit (normal discontinuous line), implicit/implicit (short discontinuous line) and is compared with the mean acceleration Newmark scheme (long discontinuous line). The results obtained compare very well with those of the explicit–implicit subcycling method proposed in Reference [9]. However, the stability of this last method is influenced by the size of the explicit elements near the implicit subdomain. Thus, if we call R the ratio between the size of these transition elements and the explicit elements with length 10, one shows that the method is stable only for $R \geqslant 10$ in the case of a time step ratio of 10 between implicit and explicit. For some values of R less than 10, one also obtains stable cases in the two examples above in the presence of numerical damping. But the algorithm is unstable in all cases when the critical value R equals 1. We use the new explicit–implicit subcycling method in the two cases above for R equals 1 and a time step ratio of 10 between implicit and explicit.

Figure 14 corresponds to the same study as in Figure 12 with a time step ratio of 10 between implicit and explicit and a ratio of 1 between the explicit interface element and the other explicit elements. The continuous line corresponds to the new method with subcycling and the discontinuous line to the reference method.

Figure 15 corresponds to the same study as in Figure 13 with a time step ratio of 10 between implicit and explicit and a ratio of 1 between the explicit interface element and the other explicit elements. The curves correspond to the new method with subcycling implicit/explicit (normal discontinuous line), implicit/implicit (short discontinuous line) and the reference method (long discontinuous line). The explicit/explicit case is detailed later since, in this case, the time step associated with the coarse time scale does not verify the CFL condition. The results lead to the following remarks:

The size of the interface finite elements is independent of the time step ratio (even without numeric damping) in all numeric scheme coupling cases (E/E, E/I, I/I). Thus, only the CFL condition needs to be verified for all explicit elements.

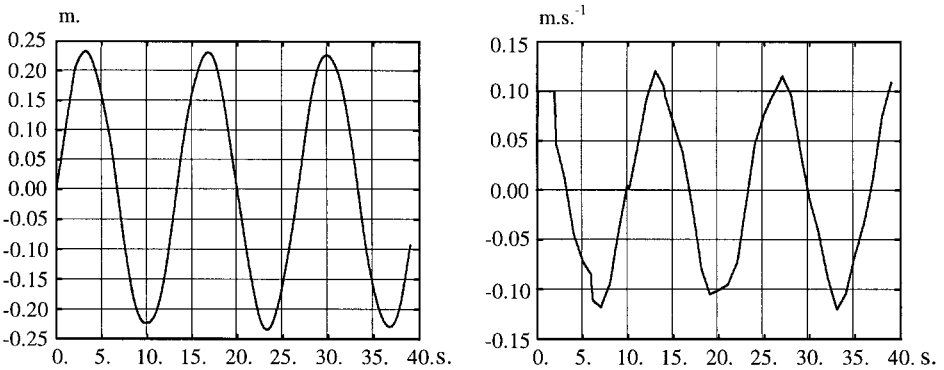

Figure 14. Horizontal displacement of the end point and horizontal velocity of the end point.

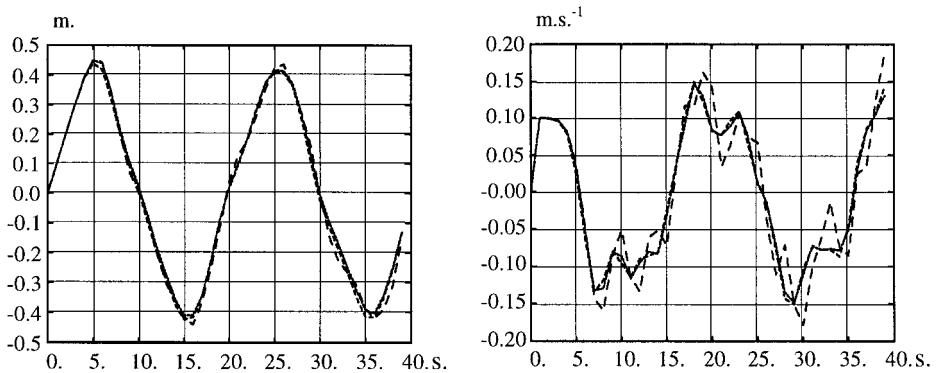

Figure 15. Horizontal displacement of the end point and horizontal velocity of the end point.

The results are identical to the reference solution for Figure 14 and the results are always better in amplitude and phase compared to the reference method in the case of Figure 15.

In the case of explicit/explicit coupling with the same Young's modulus for the three subdomains and a time step ratio of 10, we modify the test case by discretizing the central subdomain with only three finite elements. Thus, the ratio between the critical time steps is exactly equal to 10. Therefore, this test case enables us to study the coupling between explicit/explicit subdomains with subcycling when the CFL condition is verified exactly for each subdomain: the closer the time step is to the critical time step, the more precise the explicit methods will be in amplitude and phase. In the case of a beam in traction, one can show that the central difference scheme allows one to find the analytic solution exactly. The new subcycling method enables us again to find the analytical solution in displacement and velocity (see Figure 16), with the understanding that the time step is finite.

It was absolutely not obvious *a priori* that subcycling would also yield the analytical solution in this case, even though the CFL condition is verified exactly in each subdomain. Thus, the linear interpolation of velocities which allows to go from the fine time scale to the coarse time scale turns out to be exact in the case of coupling between explicit/explicit

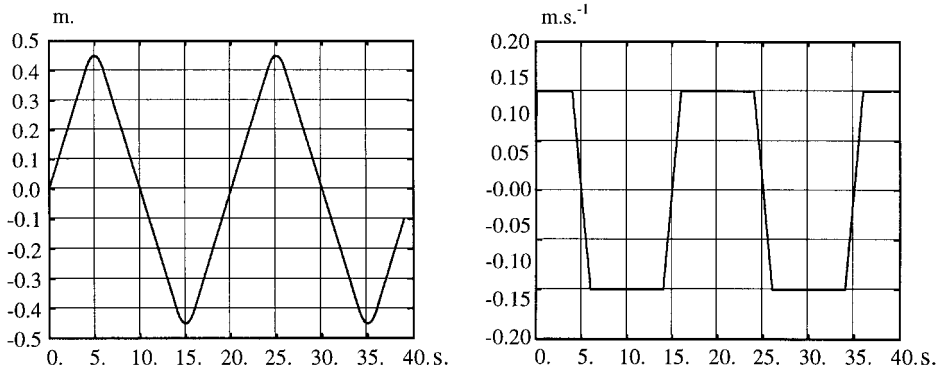

Figure 16. Horizontal displacement of the end point and horizontal velocity of the end point.

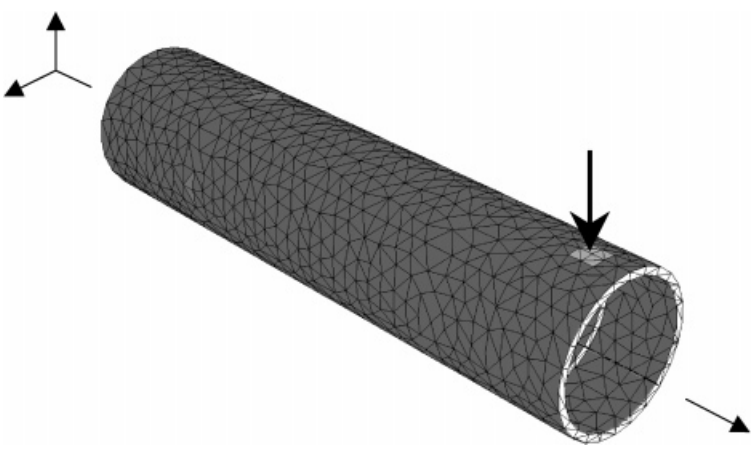

Figure 17. Structural mesh.

schemes because, in the case of the central difference numeric scheme, one can show that the acceleration is constant and the velocity linear between the discrete times. This enables us to corroborate the numerical results obtained in the case of the fixed-free beam subjected to uniform velocity. Furthermore, this remarkable result confirms the theoretical approach used in order to develop this new subcycling method.

4.5. Case of a reinforced pipe fixed at both ends and subjected to bending

In this example, we consider a pipe which is 8 m long, with 1 m radius and 5 mm thickness. This pipe also has axial and radial reinforcements (5 mm thick and 0.1 m high). The finite element model for the structure is made with DKT shell elements. The prescribed boundary conditions consist of zero displacements at both ends of the pipe and a vertical non-zero load near the edge ($F = -2 \times 10^5$ N). The inner circular stiffeners are located 1 m from the end for the first one, then every 2 m. The inner longitudinal stiffeners are placed 90° from one another (Figure 17).

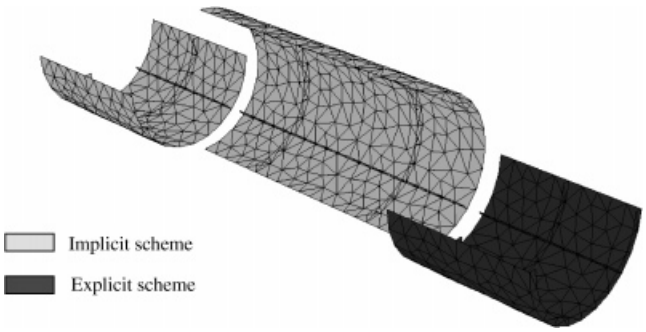

Figure 18. Exploded view showing three of the six subdomains.

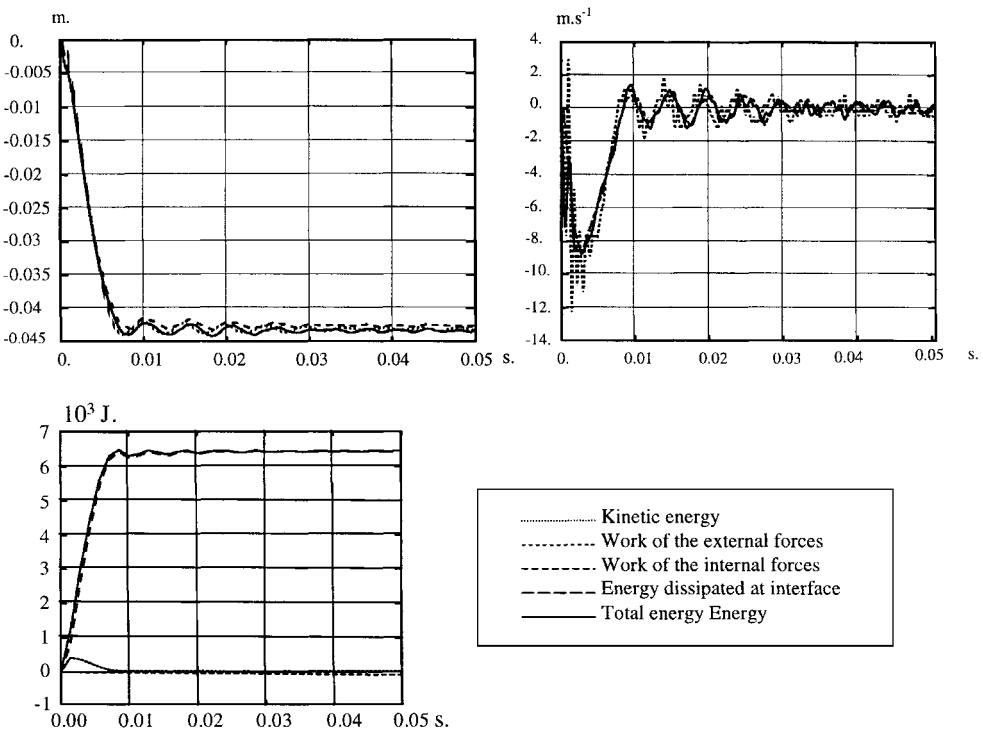

Figure 19. Vertical displacement under the loaded zone and vertical velocity under the loaded zone and energy balance.

The complete structure is decomposed into 6 subdomains of the following shapes (Figure 18):

Four out of the six subdomains are calculated with an implicit numeric scheme and the other two (including the subdomain with the loaded zone) with an explicit numeric scheme. The mesh of the complete structure consists of 8664 degrees of freedom. In this example,

algorithm	reference	E / I m=10	E / I m=100
CPU (mn)	154	41	31

Figure 20. Time comparison between the different cases.

we consider for the whole structure an elastic–plastic non-linear constitutive law with strain hardening (the mass density, Young's modulus and tangent modulus are the same as in Section 4.3, and yield stress 200 MPa). The material is standard, homogeneous isotropic steel. Furthermore, the calculation is performed taking into account large displacements. Thus, we are able to compare the vertical velocity and displacement of the structure under the loaded zone. As before, the results are compared with those of a calculation on the structure without subdomains using the Newton method coupled with the mean acceleration implicit numeric scheme. Also, we consider two time step ratios in order to study the influence of this factor on the response with time.

On the curves in Figure 19, we compare the vertical velocity and displacement obtained with time step ratios $m = 10$ (continuous line) and $m = 100$ (discontinuous line) to the reference results (short discontinuous line). The reference solution is the mean acceleration implicit scheme, which presents spurious oscillations at the beginning of the calculation. In the two cases with subcycling, these oscillations disappear because we use an explicit method with a fine time scale on the loaded zone. In the last case, the number of time steps of the implicit scheme is relatively small (35), but it allows us to obtain a satisfactory solution in amplitude as well as in phase. Figure 19 shows the energy balance of the method with subcycling in the case $m = 100$. In this case, the dissipation at the interface is 1.9 per cent. In Figure 20, the calculation times measured on the same workstation show a gain in time on the order of 5 per cent compared to the reference method.

5. CONCLUSION

We have presented a method with different time discretizations in each subdomain which allows us to couple explicit non-linear/implicit non-linear numeric schemes with time step ratios of the order of 100. The non-linearities considered are of two types: non-linear constitutive laws and geometric non-linearities (taking large displacements into account). The method was first studied and validated through two examples. Then, we showed, in the case of a fixed–fixed structure in which the non-linearities are concentrated in a defined area of the structure (explicit numeric schemes), that a gain in computation time on the order of 5 compared to a reference solution using a classical method can be achieved. This type of method is fully compatible with parallel processing, to be implemented at a later stage.

REFERENCES

1. Bonini J, Bung H. Modelisation des problèmes de contact-impact avec frottement en explicite par la méthode des multiplicateurs de Lagrange. *3ème Colloque National en Calcul des Structures.* Giens, 1997; 411–416.
2. Gayffier (de) A, Lepareux M, Bung H, Letellier A. Réflexions sur les méthodes de la dynamique explicite dans CASTEM 2000 et PLEXUS. *Rapport interne* CEA, 1996.
3. Felippa CA, Park KC. Direct integration methods in non-linear structural dynamics. *Computer Methods in Applied Mechanics and Engineering* 1979; **17-18**:277–313.

4. Gayffier (de) A, Bung H, Bonini J, Lepareux M. Dynamique explicite dans CASTEM 2000. Spécifications et développements. *Rapport interne CEA*, 1997.
5. Belytschko T, Mullen R. Explicit integration of structural problems. In *Finite Elements in Nonlinear Mechanics*, Bergen P, *et al* (eds), vol. 2, 1977; 697–720.
6. Belytschko T, Mullen R. Stability of explicit–implicit mesh partitions in time integration. *International Journal for Numerical Methods in Engineering* 1978; **12**:1575–1586.
7. Hughes TJR, Liu WK. Implicit–explicit finite elements in transient analysis: implementation and numerical examples. *Journal of Applied Mechanics* 1978; **45**:375–378.
8. Hughes TJR, Liu WK. Implicit–explicit finite elements in transient analysis: stability theory. *Journal of Applied Mechanics* 1978; **45**:371–374.
9. Liu WK, Belytschko T. Mixed-time implicit–explicit finite elements for transient analysis. *Computers and Structures* 1982; **15**:445–450.
10. Muller A, Hughes TJR. Mixed finite element methods and iterative solutions: an algorithm for structural finite element analysis. *Proceedings of the International Conference on Innovative Methods for Nonlinear Problems*, Pineridge Press International Limited: Swansea, U.K., 1984.
11. Miranda I, Ferencz RM, Hughes TJR. An improved implicit–explicit time integration method for structural dynamics. *Earthquake Engineering and Structural Dynamics* 1989; **18**:643–653.
12. Belytschko T, Mullen R. Mesh partitions of explicit–implicit time integration. *Proceedings US–Germany Symposium on Formulations and Computational Algorithms in Finite Element Analysis*, Massachussetts Institute of Technology, Cambridge, MA, 1976.
13. Hughes TJR, Pister KS, Taylor RL. Implicit–explicit finite elements in non-linear transient analysis. *Computer Methods in Applied Mechanics and Engineering* 1979; **17**(18):159–182.
14. Chen GG, Hsu TR. A mixed explicit–implicit (EI) algorithm for creep stress analysis. *International Journal for Numerical Methods in Engineering* 1988; **26**:511–524.
15. Belytschko T, Lu YY. Stability analysis of elemental explicit–implicit partitions by Fourier methods. *Computer Methods in Applied Mechanics and Engineering* 1992; **95**:87–96.
16. Sotelino ED. A concurrent explicit–implicit algorithm in structural dynamics. *Computers and Structures* 1994; **51**(2):181–190.
17. Belytschko T, Yen H-J, Mullen R. Mixed methods for time integration. *Computer Methods in Applied Mechanics and Engineering* 1979; **17**(18):259–275.
18. Liu WK, Lin J. Stability of mixed time integration schemes for transient thermal analysis. *Numerical Heat Transfer* 1982; **5**:211–222.
19. Belytschko T, Smolinski P, Liu WK. Multi-stepping implicit–explicit procedures in transient analysis. *Proceedings of the International Conference on Innovative Methods for Nonlinear Problems*, Pineridge Press International Limited: Swansea, U.K., 1984.
20. Belytschko T, Smolinski P, Liu WK. Stability of multi-time step partitioned integrators for first-order finite element systems. *Computer Methods in Applied Mechanics and Engineering* 1985; **49**:281–297.
21. Smolinski P, Belytschko T, Neal M. Multi-time-step integration using nodal partitionning. *International Journal for Numerical Methods in Engineering* 1988; **26**:349–359.
22. Smolinski P, Palmer T. Procedures for multi-time step integration of element-free Galerkin methods for diffusion problems. *Computers and Structures* 2000; **77**:171–183.
23. Smolinski P, Sleith S, Belytschko T. Stability of an explicit multi-time step integration algorithm for linear structural dynamics equations. *Computational Mechanics* 1996; **18**:236–244.
24. Belytschko T, Gilbersen ND. Implementation of mixed time integration techniques on a vectorized computer with shared memory. *International Journal for Numerical Methods in Engineering* 1992; **35**:1803–1828.
25. Daniel WJT. Analysis and implementation of a new constant acceleration subcycling algorithm. *International Journal for Numerical Methods in Engineering* 1997; **40**:2841–2855.
26. Combescure A, (de) Gayffier A, Gravouil A, Greffet N. A lagrange multiplier based domain decomposition method for time-dependent problems involving several time-scales. *IV World Congress on Computational Mechanics*, 1998.
27. Combescure A, Gravouil A. Méthode multi-échelles en temps avec décomposition de domaines pour la dynamique non-linéaire des structures. *Congrés National de Mécanique*, Giens, France, 1999.
28. Roux FX. Méthodes de résolution par sous-domaines en statique. *La recherche Aérospatiale* 1990; **1**:37–48.
29. Farhat C, Mandel C. A scalable Lagrange multiplier based domain decomposition method for time-dependent problems. *International Journal for Numerical Methods in Engineering* 1995; **38**:3831–3853.
30. Felippa CA, Park KC. A direct flexibility method. *Computer Methods in Applied Mechanics and Engineering* 1997; **149**:319–337.
31. Farhat C, Crivelli L, Géradin M. On the spectral stability of time integration algorithms for a class of constrained dynamics problems. *AIAA 34th Structural Dynamics Meeting*, 1993.
32. Ladevèze J. Algorithmes adaptés aux calculs vectoriels et parallèles pour des méthodes de décomposition de domaine. *Actes du Troisième Colloque Tendances Actuelles en Calcul des Structures*, Pluralis, 1985; 893–907.

33. Ladevèze P. *Mécanique non-linéaire des structures—Nouvelle approche et méthodes de calcul non incrémentales*. Hermès: Paris, 1996.
34. Ladevèze P, Lorong Ph. A large time increment approach with domain decomposition technique for mechanical non-linear problems. *Computer Methods in Applied Science and Engineering* 1992; 569–578.
35. Ladevèze P, Dureisseix D. Comparison of multi-level approaches in domain decomposition for structural analysis. In *Advances in Computational Mechanics with High Performance Computing*. Civil-Comp Press: Edinburgh, 1998; 55–63.
36. Kaveh A, Roosta GR. Domain decomposition for finite element analysis. *Communications in Numerical Methods in Engineering* 1997; **13**:61–71.
37. Meynen S. Domain decomposition methods for the solution of non-linear problems in solid mechanics. In *Advances in Computational Mechanics with High Performance Computing*. Civil-Comp Press: Edinburgh, 1998; 87–94.
38. Park KC, Felippa C. A variational principle for the formulation of partitioned structural systems. *International Journal for Numerical Methods in Engineering* 2000; **47**:395–418.
39. Belytschko T, Engelmann BE, Liu WK. *A Review of Recent Developments in Time Integration.* The American Society of Mechanical Engineers: New York, 1989; 185–199.
40. Newmark MN. A method of computation for structural dynamics. *Proceedings ASCE 85*, *EM3*, 1959.
41. Goudreau GL, Taylor RL. Evaluation of numerical integration methods in elastodynamics. *Computer Methods in Applied Mechanics and Engineering* 1972; **2**:69–97.
42. Zienkiewicz OC. A new look at the Newmark, Houbolt and other time stepping formulas. A weighted residual approach. *Earthquake Engineering and Structural Dynamics* 1977; **5**:413–418.
43. Herting DH. A general purpose non-linear transient integration system. *Proceedings of the International Conference on Innovative Methods for Nonlinear Problems*, Pineridge Press International Limited: Swansea, U.K., 1984.
44. Zienkiewicz OC, Wood WL, Hine NW. A unified set of single step algorithms. PART 1: General formulation and applications. *International Journal for Numerical Methods in Engineering* 1984; **20**:1529–1552.
45. Farhat C, Géradin M. On a component mode synthesis method and its application to incompatible substructures. *Computers and Structures* 1994; **51**:459–473.
46. Hughes TJR, Belytschko T. Nonlinear finite element analysis, Zace services Ltd—ICE Division, 1995.
47. Hughes TJR. Analysis of transient algorithms with particular reference to stability behavior. In *Computational Methods for Transient Analysis*, Belytschko T, Hughes TJR (eds). North-Holland: Amsterdam, 1983; 67–155.
48. Ortiz M, Simo JC. An analysis of a new class of integration algorithms for elastoplastic constitutive relations. *International Journal for Numerical Methods in Engineering* 1986; **23**:353–366.
49. Caddemi S, Martin JB. Convergence of the Newton–Raphson algorithm in elastic-plastic incremental analysis. *International Journal for Numerical Methods in Engineering* 1991; **31**:177–191.
50. Combescure A, Chavant C, Hoffmann A. Calcul linéaire et non-linéaire des coques. Cours effectué à l'ipsi. *Rapport* du département de Mécanique et Technologie 79-022, Commissariat à l'Energie Atomique, 1979.
51. Verpeaux P, Charras T, Millard A. CASTEM 2000 une approche moderne du calcul des structures. In *Calcul des structures et intelligence artificielle*, Fouet JM, Ladevèze P, Ohayon R (eds). Pluralis, 1988; 261–271.
52. Farhat C, Roux F-X. Implicit parallel processing in structural mechanics *Computational Mechanics Advances* 1994; **2**.